Journal of Orthopaedic Translation 49 (2024) 246–263

Contents lists available at ScienceDirect

Journal of Orthopaedic Translation

journal homepage: www.journals.elsevier.com/journal-of-orthopaedic-translation

Original Article

FOXO1-mTOR pathway in vascular pericyte regulates the formation of type H vessels to control bone metabolism

Caiyu Cheng [a,b,1], Mingye Deng [a,b,1], Chubin Cheng [a,b], Hangtian Wu [a,b], Yutian Wang [a,b], Mincheng Lu [a,b], Zilong Yao [a,b], Kaiqun Li [a,b], Xianrong Zhang [a,b,**], Bin Yu [a,b,*]

[a] Division of Orthopaedics and Traumatology, Department of Orthopaedics, Nanfang Hospital, Southern Medical University, Guangzhou, 510515, PR China
[b] Guangdong Provincial Key Laboratory of Bone and Cartilage Regenerative Medicine, Nanfang Hospital, Southern Medical University, Guangzhou, 510515, PR China

ARTICLE INFO

Keywords:
Bone degeneration
FOXO1
mTOR
Pericyte
Type H vessel

ABSTRACT

Background: As the population aging progresses, age-related osteoporosis has become one of the most common and severe chronic degenerative diseases. Due to insufficient understanding of its complex pathomechanisms, current clinical treatments often suffer from many negative effects. Type H vessels play critical role in bone remodeling owing to their specialized function in coupling angiogenesis and osteogenesis. Increasing evidences have shown a close association between the age-related decline of type H vessels and bone loss. However, the underlying mechanisms whereby the regression of type H vessels with aging remain largely unknown.

Methods: *Col2-Cre^{ERT}/Foxo1$^{flox/flox}$* mice and FOXO1 inhibitor (AS1842856) treated adult (6 months) and middle aged (10 months) mice were utilized for evaluating the variations in bone volume, bone microarchitecture and type H vessels through micro-CT scanning analysis, histological staining and immunofluorescence staining. *In vitro* tube-forming and scratch assays were applied to evaluate the angiogenic capacity of human umbilical vein endothelial cells (HUVECs) exposed to AS1842856 or conditioned culture milieu of Human Brain Vascular Pericytes (HBVPs). The expression of pericyte marker proteins, myofibroblast-related proteins and genes in inhibitors-stimulated HBVPs were detected via western blot analysis and Reverse transcription-quantitative PCR (RT-qPCR). Furthermore, perivascular myofibroblastic-like transformation was confirmed in AS1842856-treated animal models through immunofluorescence staining. We also constructed *Adipoq-Cre/Foxo1$^{flox/flox}$* conditional knockout mice and measured their bone mass and type H vessels by micro-CT and immunofluorescence staining. Mechanistic experiments *in vitro* were conducted via detection of mTOR signalling expression in HBVPs with pharmacological intervention (AS1842856 and rapamycin), genetic knockdown of *Foxo1*, or FOXO1-overexpression plasmid treatment, verified by RT-qPCR, western blot analysis and cellular immunofluorescence staining. *In vivo* validation was conducted on *Adipoq-Cre/Foxo1$^{flox/flox}$* mice using immunofluorescence staining. Finally, alterations in osteo-morphology and type H vessels were verified in AS1842856-treated and rapamycin-treated aged mouse models.

Results: This study identified FOXO1 in pericytes as key components for the formation of type H vessels. We found that FOXO1 expression in pericytes decreases with aging, and pharmacological blocking with AS1842856 promoted type H vessels degeneration and increased bone loss in adult and middle-aged mice, while rapamycin prevented the above pathology in middle-aged mice. We further showed that the loss of FOXO1 in *Adipoq^{+}* pericytes led to degeneration of type H vessels and bone loss in mice. Mechanistically, the inhibition of FOXO1 by AS1842856 or knockdown of *Foxo1* by siRNAs activated mTOR signaling, thereby resulting in the myofibroblastic transformation of pericytes. Furthermore, blocking mTOR signaling by rapamycin rescued the above effects *in vitro* and *in vivo*.

Conclusion: Our findings uncover a hitherto unknown role of FOXO1 in maintaining the phenotype and function of pericytes, thereby promoting formation of type H vessels. This suggests that targeting the FOXO1-mTOR

* Corresponding author. Division of Orthopaedics and Traumatology, Department of Orthopaedics, Nanfang Hospital, No. 1838, Guangzhou Avenue North, Baiyun District, Guangzhou, 510515, PR China.
** Corresponding author. Division of Orthopaedics and Traumatology, Department of Orthopaedics, Nanfang Hospital, No. 1838, Guangzhou Avenue North, Baiyun District, Guangzhou, 510515, PR China.
E-mail addresses: xianrongzh@smu.edu.cn (X. Zhang), yubin@smu.edu.cn (B. Yu).
[1] These authors contributed equally: Caiyu Cheng, Mingye Deng.

https://doi.org/10.1016/j.jot.2024.08.010
Received 9 April 2024; Received in revised form 31 July 2024; Accepted 13 August 2024
Available online 17 September 2024

pathway in pericytes could be a potential therapeutic approach to overcome the regression of type H vessels and bone degeneration with aging.

The translational potential of this article: Our research uncovers a previously unidentified role of FOXO1 in preserving pericyte characteristics and promoting the development of type H vessels. Future translational research targeting the FOXO1-mTOR pathway in pericytes may provide new strategies for the prevention and treatment of age-related osteoporosis in the clinic.

1. Introduction

The aging population is leading to an increasing incidence of age-related osteoporosis, and consequently an increase in fragility fractures [1]. Epidemiological data reveal that 10.5 % of men and 9.7 % of women aged 40 and older in China [2] and approximately 20 % of men and 50 % of women aged 50 and older in the United States [3], suffered from osteoporotic fracture, a leading cause of disability in the elderly [4]. Most approved therapies for osteoporosis have focused on either suppressing bone resorption, such as bisphosphonates and calcitonin, or promoting bone formation by targeting anabolic pathways, such as recombinant parathyroid hormone and romosozumab-aqqg [5]. However, clinical data have shown that while these medications may significantly improve trabecular bone mass, they also have serious adverse effects, limiting their safety for long-term use [6,7]. Thus, age-related osteoporosis remains a major challenge, necessitating further research to identify new therapeutic targets to prevent or halt bone degeneration.

Bone remodeling requires a subtype of capillaries characterized by strong expression of CD31 and Endomucin (Emcn), which is termed type H vessels. These capillaries locate in the metaphysis close to the chondro-osseous junction and provide crucial niches for the maintenance of osteoprogenitors and hematopoietic stem cells [8,9]. Therefore, the number of type H vessels is critical to appropriate bone modeling, remodeling, and function [8]. Increasing evidences have shown that the decline in type H vessels with age correlates with age-related bone loss [8,10,11]. However, little is known about the mechanism underlying the reduction of type H vessels with aging. Recent studies have indicated that the loss of pericyte contributes to decreased capillary density and dysfunction in the aged brain [12,13]. As perivascular mural cells of capillaries, pericytes are essential for regulating capillary integrity, diameter, and blood flow [12,14]. Indeed, evidence has shown the critical role of pericytes in coupling angiogenesis with osteogenesis during bone remodeling and repair [15]. Despite the well-established endothelial–pericyte interaction in angiogenesis, further studies are necessary to elucidate the potential role and mechanism of pericytes in bone degeneration with aging.

Forkhead box O1 (FOXO1), a key transcription factor belonging to the subfamily member O of forkhead box family, is activated under stress conditions such as growth factor depletion and high levels of ROS, thereby regulating cell metabolism, differentiation, and transformation [16,17]. FOXO1, ubiquitously expressed in mammalian tissues, including bone, plays an important role in bone metabolism. Studies in mice have indicated a critical role of FOXO1 in osteoblastic differentiation and bone formation. Conditional knock-out of FOXO1, -3, and -4 in Osterix-positive progenitors increases the number of osteoblasts and bone mass [18]. Conversely, deletion of FOXO1 in Bglap-positive osteoblasts induces bone loss in young mice but improves bone mass in old mice [19]. Previous evidence has demonstrated that vessels are sensitive to changes in FOXO1 activity in endothelial cells. Loss of FOXO1 induces a profound vessel hyperplasia and enlargement, while overexpression of FOXO1 restricts vascular expansion and leads to hypobranching [17,20]. However, the role of FOXO1 in mediating age-associated bone loss remains unknown.

Here, we report a previously unknown fundamental function of FOXO1 in maintaining the phenotype of vascular pericytes by suppressing mTOR signaling. Pharmacological inhibition and genetic deletion of FOXO1 in pericytes may lead to the pericyte-to-myofibroblast transformation and the degeneration of type H vessels in the metaphyseal bone. Since FOXO1 in pericytes is essential for bone metabolism by maintaining the formation of type H vessels in bone, deficiency of perivascular FOXO1 contributes to age-related bone loss.

2. Materials and methods

2.1. Mice models and treatments

All animal experiments were performed according to the protocols approved by the Institutional Animal Care and Use Committee (IACUC) at Southern Medical University Nanfang Hospital, and all procedures were carried out following IACUC guidelines. Male C57BL/6 mice aged 6, 10, 12 months and 8 weeks were obtained from the Experimental Animal Center at Southern Medical University, and were housed under specific pathogen-free conditions (25 °C, 12-h light/dark cycle) with free access to food and water. All mice were acclimated to our animal facility for at least one week before use in the experiments.

To investigate the role of FOXO1 in bone metabolism during aging, we treated the adult (6 months old) and middle aged (10 months old) mice with FOXO1 inhibitor (AS1842856, HY-100596, MedChemExpress) at dose of 30 mg/kg per day, 5 days per week, or an equal volume of vehicle by oral gavage. After 2 months of treatment, mice at 8 and 12 months old were euthanized, and bilateral tibiae and femora were harvested for further analysis. To evaluate the role of mTOR signaling in vessel degeneration in bone, 12-month-old mice received 2 mg/kg rapamycin (HY-10219, MedChemExpress) by intraperitoneal injection on alternate days, while control mice were treated with the same volume of saline. After 4 weeks of treatment, mice were euthanized, tibiae and femurs were collected for further analysis.

To investigate the role of FOXO1 in bone metabolism, we crossed *Col2-Cre^{ERT}* mice (RRID: IMSR_JAX: 006774) with *Foxo1$^{flox/+}$*mice (Quote: TOS191231MG2-B, Stock No. 017986, Cyagen Bioscience Inc. China) to generate *Col2-Cre^{ERT}/Foxo1$^{flox/flox}$* mice. Ten-month-old *Col2-Cre^{ERT}/Foxo1$^{flox/flox}$* mice were injected intraperitoneally with tamoxifen (CAS# 10540-29-1, Sigma–Aldrich) at 75 mg/kg once a day for 5 consecutive days. After 8 weeks of treatment, mice were euthanized, and femurs were collected for further analysis.

Considering that Adiponectin expressing cells (*Adipoq^{+}*) are as abundant as both pericytes and stromal cells in the bone marrow [21], we crossed *Adipoq-Cre* mice (RRID: IMSR_JAX: 010803) with *Foxo1$^{flox/flox}$* mice, to investigate the role of FOXO1 in vasculature maintenance. The *Adipoq-Cre/Foxo1$^{flox/flox}$* mice and *Foxo1$^{flox/flox}$* mice in the same littermates were euthanized at 4 weeks of age, and femurs were harvest for comparative analysis. PCR analyses of genomic DNA were used to determine the genotypes of the mice using the following primers: Col2-Forward: 5'-cactgcgggctctacttcat-3', Col2-Reverse: 5'-accagcagcacttttggaag-3'; Adipo-Forward: 5'-acggacagaagcattttcca-3', Adipo-Reverse: 5'-ggatgtgccatgtgagtctg-3'; LoxP (Foxo1)-Forward: 5'-gctttcttctaatgccatctggtt-3', LoxP (Foxo1)-Reverse: 5'-tattttagagctggcagaaagcac-3'.

2.2. Micro-computed tomography (micro-CT) analysis

For micro-CT analysis, femurs were obtained from mice, dissected free of soft tissue, fixed in 4 % paraformaldehyde for 24 h, and subsequently scanned by Bruker Micro-CT Skyscan 1276 system (Bruker, Kontich, Belgium). Scanning was performed with a voxel size of 5 μm, a

voltage of 85 kV, a current of 200 mA, 1 mm Al filter and an integration time of 384 ms. Density measurements were calibrated using the manufacturer's calcium hydroxyapatite (CaHA) phantom. Reconstruction was performed using NRecon software (version 1.7.4.2, SkyScan, Bruker). 3D images were obtained from contoured 2D images by methods based on distance transformation of the grayscale original images (CT vox; version 3.3.0, Bruker). Both 3D and 2D analyses were performed using software CT Analyser (version 1.18.8.0, Bruker). Analyses of the bone micro-architecture were carried out in a region of interest (ROI). The ROI of cancellous bone was defined as the area 0.45 mm from the epiphyseal growth plate with a length of 2 mm in the distal femora. A length of 1 mm ROI of the cortical bone was at the femoral mid-diaphysis 2.5 mm away from the distal growth plate. The parameters, including bone mineral density (BMD), trabecular bone volume fraction (BV/TV), trabecular number (Tb. N), trabecular thickness (Tb. Th), trabecular separation (Tb. Sp), trabecular bone pattern factor (Tb. Pf), cortical cross-sectional bone area (Cs. B. Area), and cortical cross-sectional thickness (Cs. Th) were calculated.

2.3. Histochemistry and immunohistochemistry analyses

Femurs were dissected free from attached muscle, and fixed overnight in 10 % formalin at 4 °C. After washing three times with ice-cold PBS, samples were decalcified at 4 °C using 10 % EDTA (pH 8.0) for 14 days, and finally processed for paraffin embedding. Coronal sections at 4-μm-thick were cut and processed for staining.

For hematoxylin and eosin (H&E) staining, bone sections were processed according to the standard protocols. Briefly, sections were stained by hematoxylin for 2 min and by eosin for 10 s.

For immunohistochemistry staining, after being deparaffinized, rehydrated and washed, sections were processed for heat-induced antigen retrieval (Tris–EDTA Buffer, pH 9.0). Sections were then incubated with 3 % hydrogen peroxide for 15 min to eliminate endogenous peroxidase activity, followed by incubation with 10 % goat serum (Cat. SL038, Solarbio, China) for 1 h to block unspecific antigens. Then, the sections were incubated with primary antibody against osteocalcin (Cat. ab93876, Abcam) overnight at 4 °C. Next day, after wash with PBST (PBS containing 0.1 % Triton X-100) for 3 times, sections were incubated with biotinylated secondary antibodies and Vectastain avidin and biotinylated horseradish peroxidase macromolecular complex (ABC) reagent (Cat. AK-5000, Vector Laboratories, Burlingame, USA) according to the manufacturer's protocol. Immunoreactivity was assessed using a diaminobenzidine (DAB) substrate kit (Cat. SK4100, Vector Laboratories, Burlingame, USA). A microscope (BX63; Olympus, Tokyo, Japan) was used for observation and imaging to detect immunoreactivity. The number of positive-stained cells was calculated with Image J software (version 1.8.0, National Institutes of Health, Bethesda, MD, USA).

The activity of osteoclasts was detected by tartrate-resistant acid phosphatase (TRAP) staining kits (Cat. No. 294–67001, Wako, Japan) following the manufacturers' instructions. In brief, rehydrated sections were incubated in TRAP staining solution in a moist chamber at room temperature for 10～30 min. TRAP-positive multinucleated cells with at least three nuclei were counted under a microscope (BX63; Olympus, Tokyo, Japan).

2.4. Immunofluorescence analysis

For immunofluorescence staining, femoral samples were fixed with 4 % paraformaldehyde overnight, decalcified with daily changes of 10 % EDTA (pH 7.5) for 6 days, and incubated in 30 % sucrose overnight prior to embedding in optimal cutting temperature (OCT) compound (Cat. BL557A, Biosharp, China). Sections at 10-μm thickness of frozen-embedded samples were prepared for staining. Frozen sections were rewarmed and washed twice in PBS buffer containing 0.1 % Triton X-100 (Cat. T8200, Solarbio, China) for 10 min per time. After being blocked with 10 % goat serum for 1 h at room temperature, sections were incubated with primary antibodies overnight at 4 °C. Sections were then washed 5 times in PBS and then incubated with a secondary antibody for 1 h at room temperature in the dark. Nuclei were counterstained with 4',6-diamidino-2-phenylindole (DAPI, Cat. E607303-0002, BBI Life Science, China). All sections were observed and imaged under a Zeiss LSM980 confocal microscope (Carl Zeiss, Germany), and the acquired images were analyzed using ZEN software (ZEN blue, Carl Zeiss).

For immunofluorescence in cell cultures, HBVPs were seeded at 1×10^6 cells per dish in confocal 35-mm glass-bottomed petri dishes. When reaching 70 % confluency, cells were treated with 50 nM *Foxo1*-siRNA, 20 nM Rapamycin, or the same volume of vehicle. After 48 h of treatment, cells were washed three times with PBS buffer, fixed with precooled 4 % paraformaldehyde solution for 20 min at room temperature, permeabilized with 0.5 % v/v Triton X-100 (PBST), blocked in 5 % goat serum, and incubated with primary antibodies. After washing, cells were incubated with secondary antibodies. Images were acquired using a confocal microscope (Zeiss LSM980, Carl Zeiss, Germany). Three fields per well were randomly chosen, and quantitative data were obtained from at least three independent experiments.

The antibodies used for immunofluorescence were Rabbit anti-CD31 (1:200, #ab28364 Abcam), Rat anti-Endomucin (1:50, #sc-65495, Santa Cruz Biotechnology), Rabbit anti-FOXO1 (1:200, #18592-1-AP, Proteintech, China), Mouse anti-αSMA (1:400, #67735-1-Ig, Proteintech, China), Rabbit anti-αSMA (1:200, #14395-1-AP, Proteintech, China), Mouse anti-PDGFRβ (1:200, #ab69506, Abcam), Mouse anti-Phospho-mTOR (1:200, #67778-1-Ig, Proteintech, China), Rabbit anti-Phospho-mTOR (1:500, #80596-1-RR, Proteintech), Mouse anti-PDGFRα (1:200, #60045-1-Ig, Proteintech), Goat anti-Rabbit IgG Alexa Fluor™ 488 (1:200, #A-11008, Invitrogen), Goat anti-Rat IgG Alexa Fluor™ 594 (1:200, #A-11007, Invitrogen), Goat anti-Mouse IgG Alexa Fluor™ 647 (1:200, #A-21235, Invitrogen).

2.5. Serum P1NP and CTX-1 assays

Mice were anesthetized, and then a cardiac puncture was performed to collect whole blood. The blood was allowed to coagulate at room temperature for 2 h, followed by centrifugation for 15 min at 1000 × *g*. Serum was then separated immediately and stored in aliquots at −80 °C for further analysis. Biochemistry assays were performed with the Mouse Procollagen I N-Terminal Peptide (P1NP) ELISA Kit (Cat. CSB-E12775m, CUSABIO, China) and Mouse cross linked C-telopeptide of type I collagen (CTX-1) ELISA Kit (Cat. CSB-E12782m, CUSABIO, China). According to the manufacturer's instructions, absorbance was measured at 450 nm, and concentrations were calculated based on a standard curve fitted by the software (CurveExpert, Version 1.40, Microsoft Corporation).

2.6. Cell culture and conditional culture

The HBVPs and HUVEs cell lines were purchased from Zhongqiaoxinzhou Biological Technology Co., Ltd (Shanghai, China). For single culture, HBVPs were grown in pericyte medium (PM, Cat. #1201, ScienCell). HUVEs were cultured in DMEM medium (#11995, Gibco) containing 2 % FBS (fetal bovine serum, Gibco) and 100 U/mL penicillin-streptomycin (#15140-122, Thermo Fisher Scientific).

For conditional culture of HUVECs, the supernatant of HBVPs culture treated with various concentrations (0, 0.1 and 1 μM) of AS1842856 (HY-100596, MedChemExpress) for 48 h were collected. The supernatants were centrifugated at 1000 rpm for 5 min to remove large cell debris and subsequently filtered through a 0.22-μm filter. The filtered supernatants were then mixed with DMEM complete medium at ratio of 1:1 (v/v) and used as conditioned medium for HUVECs.

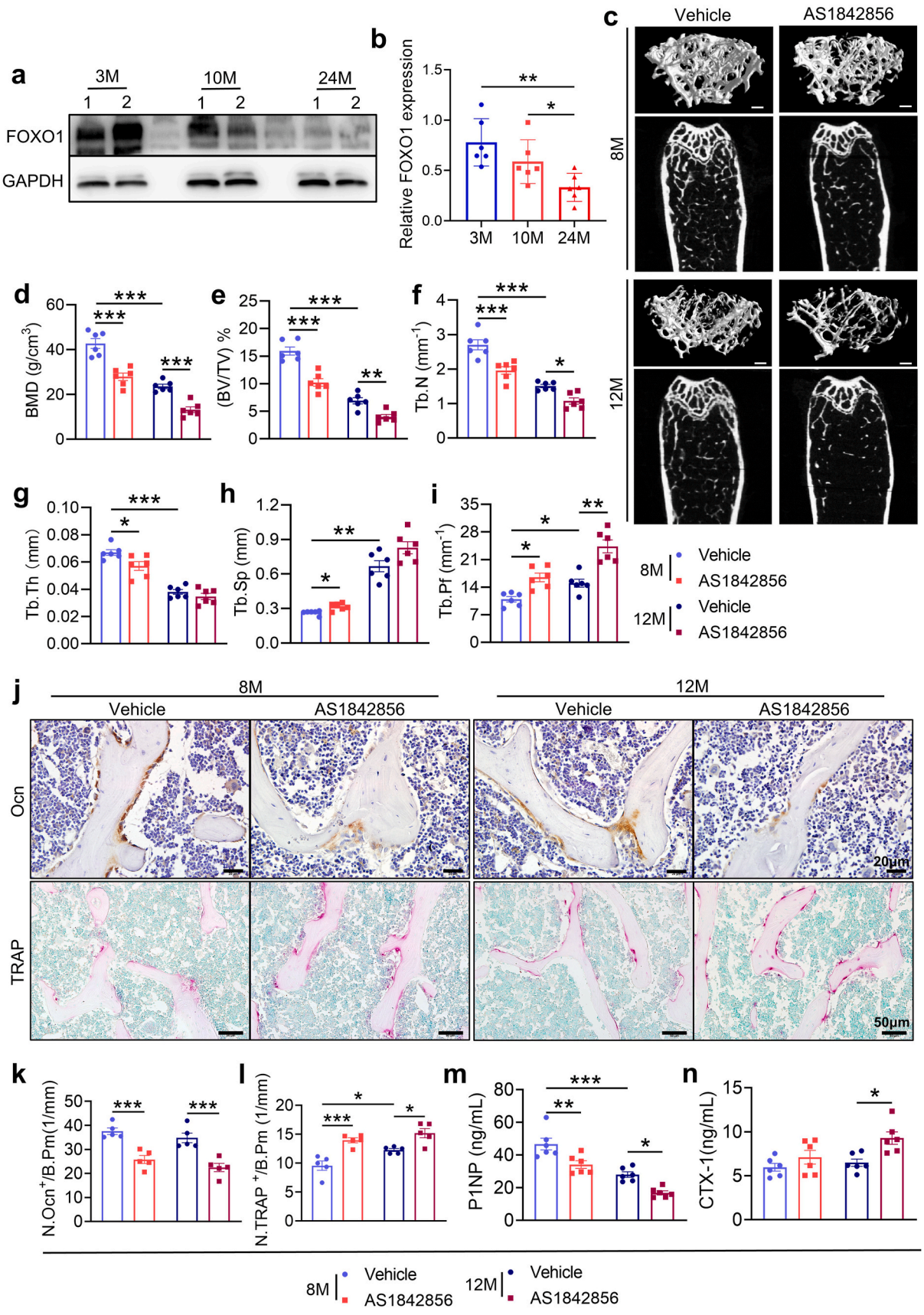

(caption on next page)

Figure 1. FOXO1 expression decreases with age and AS1842856 treatment may aggravate bone loss in mice. a, b. Western blotting (a) and quantitative analysis (b) of FOXO1 expression in tibias of 3-, 10- and 24-month-old mice. n = 6/group. *$P < 0.05$; **$P < 0.01$. **c.** Representative microcomputed tomography (micro-CT) images of the distal femur and trabeculae after 2 months of treatment with FOXO1 inhibitor (AS1842856, 30 mg/kg, 5 days of continuous gavage with 2 days interval) in 8- and 12-month-old mice. Scale bars represent 200 μm. **d-i.** Quantitative analysis of three-dimensional structural parameters, including bone mineral density (BMD) (d), trabecular bone volume fraction (BV/TV) (e), trabecular number (Tb. N) (f), trabecular thickness (Tb. Th) (g), trabecular separation (Tb. Sp) (h), and trabecular pattern factor (Tb. Pf) (i). n = 6/group. *$P < 0.05$, **$P < 0.01$, ***$P < 0.001$. **j.** Representative images of immunohistochemical staining (upper panel) for osteocalcin (Ocn) and tartrate-resistant acid phosphatase (TRAP) staining (lower panel) in the femoral metaphysis of 8- and 12-month-old mice after 2 months of AS1842856 treatment. Scale bars: 20 μm (upper panel), 50 μm (lower panel). **k.** Quantitative analysis of osteocalcin-positive (Ocn^+) cells on the surface of bone trabeculae (N. Ocn^+/mm). n = 5/group. ***$P < 0.001$. **l.** Quantitative analysis of $TRAP^+$ cells per bone surface (N. $TRAP^+$/mm). n = 5/group. *$P < 0.05$, ***$P < 0.001$. **m, n.** Serum bone formation marker P1NP (m) and resorption marker CTX-1 (n). n = 6/group. *$P < 0.05$, **$P < 0.01$, ***$P < 0.001$. Data are represented as mean ± SEM. Each data point represents one animal. Statistical comparisons were made using one-way ANOVA with Tukey's *post-hoc* test if variances were equal (b, d, e, f, g, k, l, m and n); otherwise, Dunnett's T3 test was utilized (h and i).

2.7. Tube formation assay

Chilled 24-well plates were coated with 150 μL Matrigel (Cat. # 356234; Corning) that was polymerized at 37 °C for 30~60 min. HUVECs (6×10^4 cells/well) were serum-starved overnight, trypsinized, and seeded in Matrigel-coated well with low serum (1 % fetal bovine serum). To evaluate whether blocking FOXO1 in HUVECs might influence its tube formation, we treated the HUVECs with various concentrations (0, 0.1 and 1 μM) of AS1842856. The formation of tubes was imaged on an inverted microscope (Olympus IX-73, Japan) after 12 h of treatment. To determine whether blocking FOXO1 in HBVPs might affect the tube formation of HUVECs, we treated HUVECs with the conditioned media collected from HBVPs treated with various concentrations (0, 0.1 and 1 μM) of AS1842856. Tube formation was captured on the inverted microscope at the indicated time points. Images were processed using the Angiogenesis Analyzer Program for ImageJ (version 1.8.0, NIH, USA) to obtain the total branching points and total tube length.

2.8. Scratch assay

HUVECs were cultured in 35-mm petri dishes at a density of 1×10^6 cells per dish and incubated at 37 °C for 24 h. When cells reached a 90 % confluent monolayer, a 200-μL sterile tip was used to scratch a fixed-width gap in the cell monolayer. After washing away cell debris with PBS, cells were then incubated in conditioned media. Scratch closure was monitored under an inverted microscope (Olympus IX-73, Japan) at 0, 24, 48, and 72 h after scratching. The area the scratch was detected by ImageJ software (version 1.8.0, NIH, USA) and the healing rate was calculated to assess the migration ability of the HUVECs. The healing rate was calculated as follows: wound-healing rate (%) = $(A_0 - A_n)/A_0 \times 100$ %, where A_0 and A_n represents the initial area and unhealed area of the wound, respectively.

2.9. RNA isolation and quantitative real-time PCR (qPCR) analysis

Total RNA of cells was extracted using AG RNAex Pro Reagent (#AG21101, Accurate biology, China) according to the manufacturer's instructions. Reverse transcription into cDNA was performed using Hifair® III 1st Strand cDNA Synthesis SuperMix for qPCR (#11141ES60, Yeasen, China). qPCR was performed using SYBR Green (#11202ES08, Yeasen, China) on a QuantStudio5 system (Applied Biosystems, USA) according to the manufacturer's protocol. The GAPDH genes were used as an internal control. The relative amount of each gene was calculated using the 2-ΔΔCT method. PCR primers for samples from HBVPs were h-GAPDH Forward, 5'-cagcctcaagatcatcagca-3', Reverse, 5'-tgtggtcatgagtccttcca-3'; h-VEGF Forward, 5'-gccttgccttgctgctctac-3', Reverse, 5'-tgattctgccctcctccttctg-3'; h-ANG-1 Forward, 5'-agaaccttcaaggcttggttac-3', Reverse, 5'-ggtggtagctctgtttaattgct-3'; h-PDGFRβ Forward, 5'-tgatgccgaggaactattcatct-3', Reverse, 5'-tttcttctcgtgcagtgtcac-3'; h-ACTA2 Forward, 5'-aaaagacagctacgtgggtga-3', Reverse, 5'-gccatgttctatcgggtacttc-3'; h-COL1A1 Forward, 5'-gagggccaagacgaagacatc-3', Reverse, 5'-cagatcacgtcatcgcacaac-3'; h-TAGLN2 Forward, 5'-atcccaactggttccctaagaa-3', Reverse, 5'-cccatctgtaacccgatcacg-3'; h-LOXL1 Forward, 5'-ggctgctatgacacctacaatg-3', Reverse, 5'-gtagtgaatgttgcatctcacca-3'; h-FOXO1 Forward, 5'-ggatgtgcattctatggtgtacc-3', Reverse, 5'-tttcgggattgcttatctcagac-3'; h-FOXO3a Forward, 5'-tcacgcaccaattctaacgc-3', Reverse, 5'-cacggcttgcttactgaagg-3'; h-FOXO4 Forward, 5'-ggctgccgcgatcatagac-3', Reverse, 5'-ggctggttagcgatctctgg-3'; h-FOXO6 Forward, 5'-gagttcgtggtggatgctga-3', Reverse, 5'-gcttcttcttgctcgccttg-3'.

2.10. Western blot analysis

Total protein extracts from bone tissue or cells were prepared using radio immunoprecipitation assay lysis buffer (#PC101, Epizyme, Shanghai, China) containing protease inhibitor (#HY-K0010, MedChemExpress) and phosphatase inhibitor (#HY-K0023, MedChemExpress). Protein concentrations were quantified using a Pierce Bicinchoninic Acid protein assay kit (#23225, Thermo Fisher Scientific). Proteins were resolved by SDS-PAGE and transferred to a polyvinylidene difluoride membrane (#IPVH00010, Immobilon P, Merck Millipore, Cork, Ireland). After being blocked in 5 % milk powder in TBST (Tris-buffered saline TBS buffer + 1 % Tween20) at room temperature for 1 h, the membranes were incubated with primary antibody at 4 °C overnight. The primary antibodies included Rabbit anti-β-Tubulin (1:5000, #10094-1-AP, Proteintech), Mouse anti-GAPDH (1:5000, #60004-1-Ig, Proteintech), Rabbit anti-FOXO1 (1:2000, #18592-1-AP, Proteintech), Mouse anti-PDGFRα (1:2000, #60045-1-Ig, Proteintech), Mouse anti-PDGFRβ (1:2000, #ab69506, Abcam), Mouse anti-αSMA (1:2000, #14395-1-AP, Proteintech), and Mouse anti-Phospho-mTOR (1:2000, #67778-1-Ig, Proteintech). The following day, membranes were washed three times in TBST, followed by incubation with horseradish peroxidase (HRP)-conjugated secondary antibody at room temperature for 1 h. The secondary antibodies were goat anti-mouse HRP (#HA1006, Huabio, China) and goat anti-rabbit HRP (HA1001, Huabio, China). Immunoblots were developed using Western Lightning Plus enhanced chemiluminescence (ECL) (#NEL105001EA, PerkinElmer, MA, USA), visualized and imaged using a chemiluminescence instrument (Guangzhou Ewell Bio-Technology, Guangzhou, China).

2.11. Plasmid transfection

The cDNA of human *Foxo1* gene, based on NCBI Reference Sequence NM_002015.4, was cloned into the pcDNA3.1 vector to construct *Foxo1*/pcDNA3.1 for *Foxo1* overexpression studies. The construction of *Foxo1*/pcDNA3.1 (#BW2266, BVA01) was prepared by Umine Biotechnology Co. LTD, Guangzhou. The primer sequences used for plasmid construction were: forward, 5'-atccgccaccatggccgaggcgcctcag-3'; reverse, 5'-ctcgaggcctgacacccagctatgtgtcg-3'. For plasmid transfection, HBVPs were seeded in 6-well plates at a density of $0.5 \sim 1 \times 10^6$/well. When the growth confluence reached 70~80 %, cells were transfected with *Foxo1*/pcDNA3.1 or pCDNA3.1 (control) using Lipofectamine 3000 (Invitrogen, Thermo Fisher Scientific). After 48 h of transfection, cells were used for Western blot analysis.

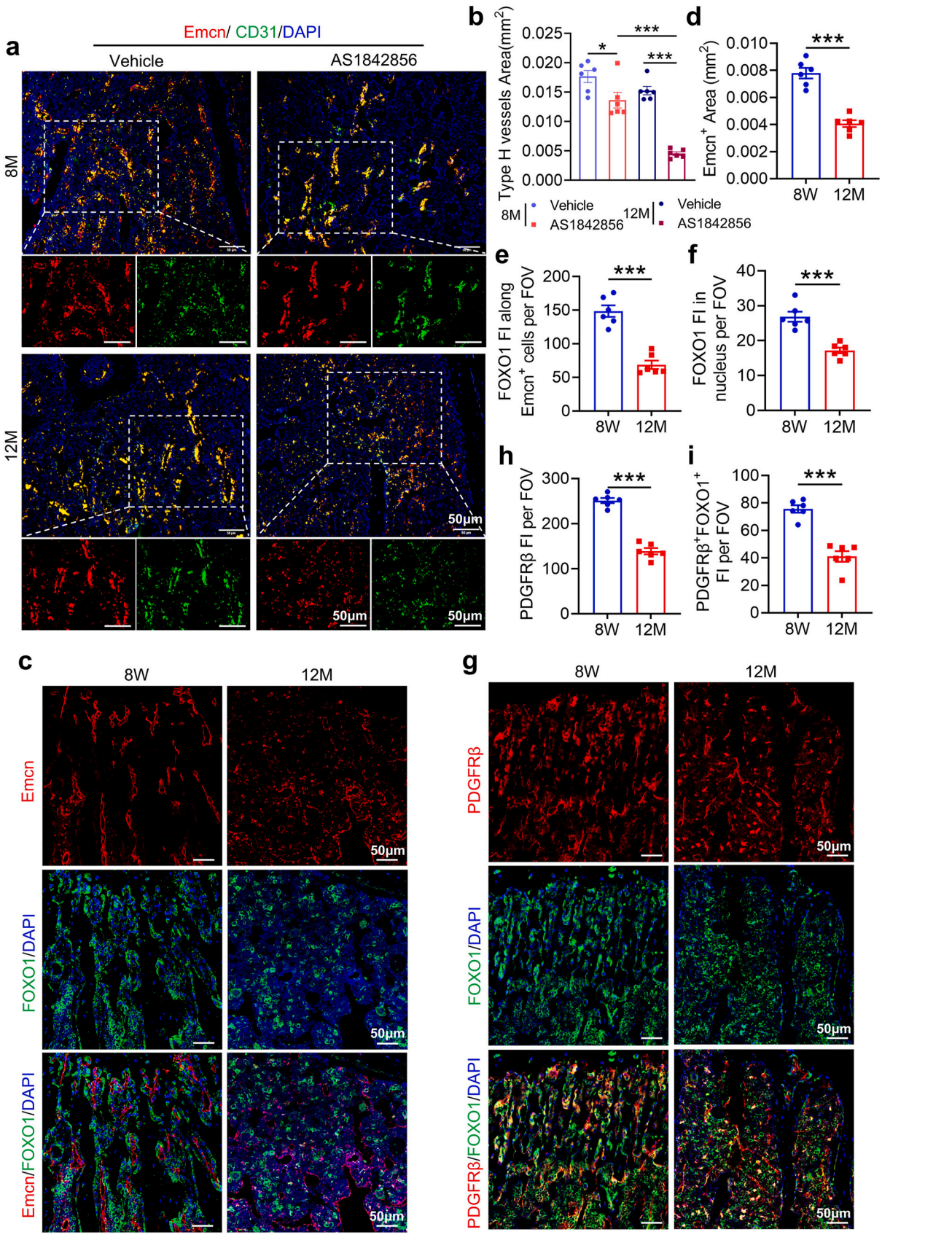

(caption on next page)

Figure 2. FOXO1 inhibition by AS1842856 exacerbates degeneration of type H vessels in the long bone of mice. a. Representative images of immunofluorescent staining of type H vessels in the femoral metaphysis of 8-month-old (8M) and 12-month-old (12M) mice treated with AS1842856 or vehicle. Scale bars represent 50 μm. **b.** Quantitative statistical plots of the fluorescent signal of type H vessels (area mm^2). n = 6/group. $^*P < 0.05$, $^{***}P < 0.001$. **c.** Representative images of the fluorescence distribution of FOXO1 around the $Emcn^+$ vessels in the metaphyseal area below the growth plate in distal femurs of mice at 8W and 12M of age. Scale bars represent 50 μm. **d-f.** Quantitative analysis of $Emcn^+$ area in metaphyseal region below the growth plate (d), relative fluorescence intensity (FI) of FOXO1 surrounding $Emcn^+$ vessels (e), and relative FI of nuclear-localized FOXO1 (f). n = 6/group. $^{***}P < 0.001$. **g-i.** Representative images (g) and quantitative analysis (h and i) of the fluorescence intensity of co-localized PDGFRβ and FOXO1 in the femoral metaphysis of mice at 8W and 12M of age. Scale bars: 50 μm. n = 6/group. $^{***}P < 0.001$. Data are represented as mean ± SEM. Each data point represents one animal. Student's *t*-test was used for the statistical analysis of two groups (d, e, f, h and i). One-way ANOVA with Tukey's *post-hoc* test was used for the statistical analysis in four groups (b).

2.12. siRNA transfection

Negative control siRNAs (siNC) and *Foxo1*-specific siRNAs were obtained from GenePharma (Shanghai, China). The sequences of *Foxo1*-targeting siRNAs were 5'-uuacuguuguuguccauggtt-3' (si-*Foxo1*#1); 5'-auaguacuagcauuugagctt-3' (si-*Foxo1*#2); 5'-uugucuugacacuguguggtt-3' (si-*Foxo1*#3) and 5'-uuaucucagacagacugggtt-3' (si-*Foxo1*#4). HBVPs at confluency of 50∼70 % were transfected with siRNAs using the Lipofectamine 3000 (Invitrogen, Thermo Fisher Scientific) following the manufacturer's protocol. Six hours after transfection, the medium was replaced with fresh medium, with or without rapamycin (20 nM). Cells were collected for subsequent experiments 48 h after transfection.

2.13. Statistical analysis

Statistical analyses were performed using SPSS 19.0 software (IBM, USA). Values in graphs were expressed as means ± SEM. Levene's test examined variance homogeneity of data to confirm the normality and homogeneity. For two-group comparisons, unpaired Student's *t*-test (equal variances) or Mann–Whitney U test (unequal variances) was used to evaluate the statistical difference. For multiple group comparisons, one-way analysis of variance (ANOVA) was used, and the differences between groups were evaluated using *post hoc* multiple comparisons with Tukey test. However, Dunnett T3's test was applied when the populations variances were not equal. A value of $P < 0.05$ was used as the criterion for statistical significance.

3. Results

3.1. FOXO1 inhibition aggravates bone loss in mice

To investigate the role of FOXO1 in bone metabolism, we first examined the protein levels of FOXO1 in tibiae of mice at 3, 10, and 24 months of age. Western blot results showed that the FOXO1 levels in 24-month-old mice were dramatically decreased relative to 3- and 10-month-old mice (Fig. 1a and b). We then treated adult and middle-aged mice with AS1842856, an inhibitor of FOXO1 for 2 months. Micro-CT analysis and three-dimensional reconstruction of trabecular bone in the distal femur revealed a decrease in BV/TV in 12-month-old mice compared with 8-month-old ones (Fig. 1c and e). The reduction in bone mass was principally due to decreased trabecular number (Tb. N) and trabecular thickness (Tb. Th) (Fig. 1f and g), alongside increased trabecular separation (Tb. Sp) and trabecular pattern factor (Tb. Pf) (Fig. 1h and i). Importantly, AS1842856 treatment exacerbated reductions in both BMD and BV/TV in 8- and 12-month-old mice (Fig. 1d and e). The decreased BV/TV by AS1842856 treatment was mainly attributed to reduced Tb. N rather than Tb. Th (Fig. 1f and g). AS1842856 treatment increased Tb. Sp only in 8-month-old mice but increased Tb. Pf in the bone in both 8- and 12-month-old mice (Fig. 1h and i). In contrast, micro-CT analysis of the femur diaphysis showed no differences in cortical thickness or cortical bone cross-sectional area (Supplementary Fig. S1a-c). To further explore the cellular mechanism that might mediate the bone loss induced by AS1842856, we performed immunohistochemical staining for Ocn, an osteoblastic marker, and histochemistry staining for TRAP, an osteoclastic marker. Results showed that AS1842856 treatment reduced the number of Ocn positive-stained cells on the surface of trabecular bone, while increased the number of TRAP positive-stained cells in the bone in both 8- and 12-month-old mice (Fig. 1j–l). In consistent, 12-month-old mice had lower level of P1NP, a bone formation marker, compared with 8-month-old mic, and AS1842856 treatment further decreased serum P1NP levels in both age groups (Fig. 1m). Additionally, AS1842856 treatment significantly increased the level of bone resorption marker CTX-1 in 12-month-old mice, with no effect observed in 8-month-old mice (Fig. 1n). These results indicate that decreased expression levels of FOXO1 may contribute to the age-related bone loss and that pharmacological blocking FOXO1 with AS1842856 may aggregate bone loss by suppressing anabolism while promoting catabolism of trabecular bone.

Given that type II collagen (Col2)-positive cells, defined as skeletal stem cells, chondrogenic and osteoblastic linage cells, contribute to both bone development and metabolism [22], we constructed *Col2*-Cre^{ERT}/$Foxo1^{f/f}$ conditional knockout (CKO) mice to investigate the function of FOXO1 in bone metabolism. *Foxo1* was knocked out in these mice at 10 months of age following tamoxifen induction. Unexpectedly, we found that knock out of *Foxo1* in $Col2^+$ cells had no effect on bone mass or the microstructure of trabecular and cortical bone in the femurs of CKO mice (Supplementary Fig. S2a-i). These data suggest that FOXO1 in $Col2^+$ cells may not be essential for trabecular or cortical bone metabolism in older mice.

3.2. FOXO1 inhibition exacerbates the degeneration of type H vessels

Type H vessels ($CD31^{hi}Emcn^{hi}$ vessels) are thought to be intimately associated with the bone metabolic microenvironment [23]. Thus, we applied immunofluorescence double staining to label type H vessels in femoral tissues from 8- and 12-month-old mice after AS1842586 treatment. The results exhibited that inhibition of FOXO1 decreased the number of H-type vessels (yellow) in both 8- and 12-month-old mice, with a 22.83 % reduction in type H vessels area in 8-month-old mice bone and a more pronounced 70.29 % reduction in 12-month-old mice (Fig. 2a and b). To investigate whether the reduction in type H vessels might be associated with the down-regulated expression of FOXO1 in endothelial cells, we performed double-fluorescence staining to show the localization of FOXO1 and Emcn. We found a distinct localization of $Emcn^+$ and $FOXO1^+$ cells, with some $FOXO1^+$ cells located closely to $Emcn^+$ cells. Notably, there was a significant decline in $Emcn^+$ cells in the femoral metaphysis of 12-month-old mice relative to 8-week-old mice (Fig. 2c and d). Furthermore, a notable loss of $FOXO1^+$ cells around $Emcn^+$ vessels and in cell nuclei was evident in the femoral metaphysis of 12-month-old mice (Fig. 2c, e, and f). Interestingly, we found that FOXO1 was colocalized with PDGFRβ, a marker for pericyte of vessels, and both the total PDGFRβ expression and the FOXO1 expression in $PDGFR\beta^+$ cells declined dramatically with aging (Fig. 2g–i). These data indicate that the reduction in FOXO1 levels in pericytes of vessels contributes to the degeneration of type H vessels.

3.3. FOXO1 inhibition in pericytes hinders angiogenesis

To evaluate the role of FOXO1 in angiogenesis, we first stimulated HUVECs with different concentrations of AS1842856. Scratch wound healing assays showed that the migration ability of HUVECs was enhanced with increasing inhibitor concentration (Supplementary Fig.

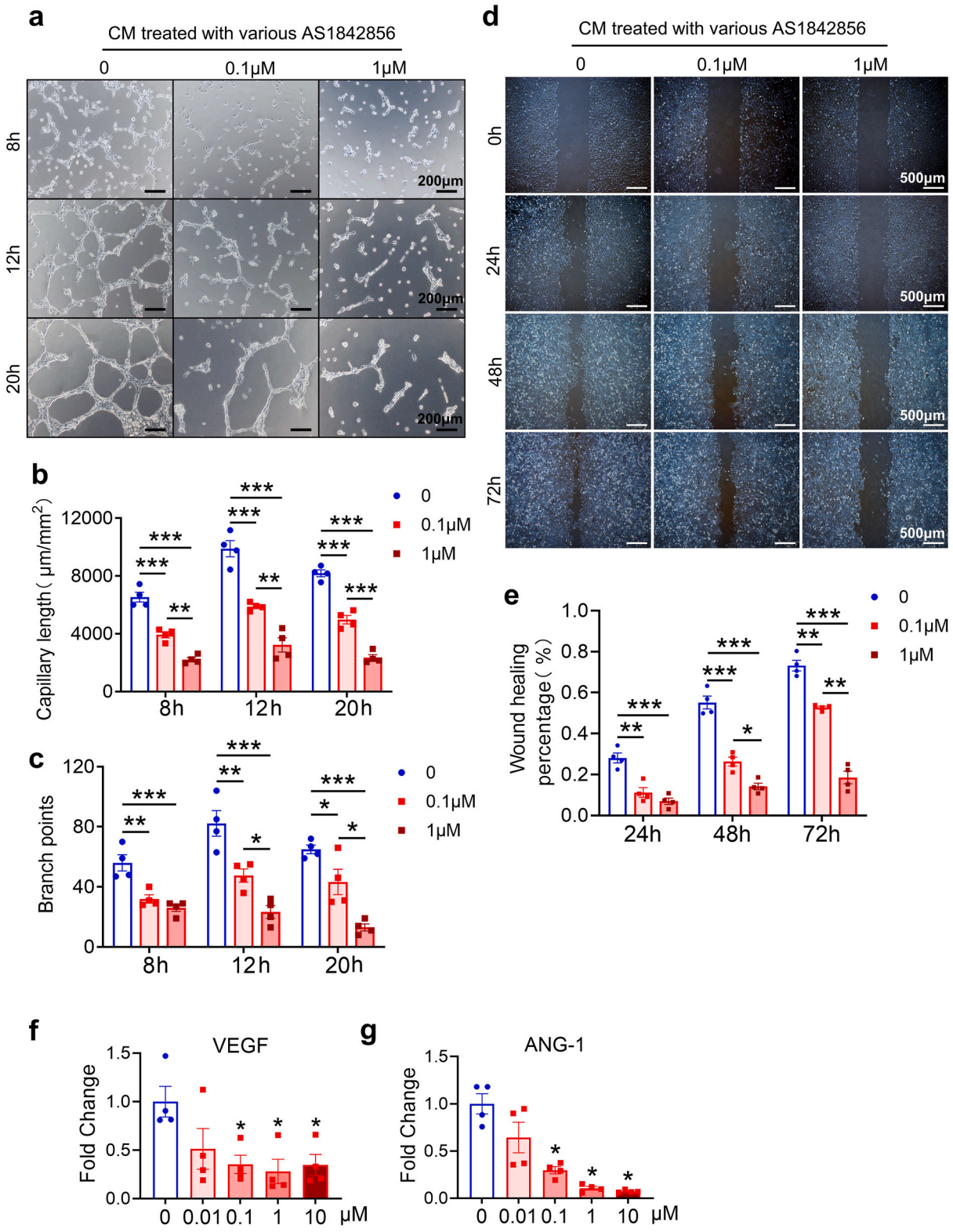

Figure 3. FOXO1 inhibition in pericytes prevents angiogenesis. a-c. Representative images (a) and quantitative analyses (b and c) of tube-forming assays of HUVECs. HUVECs were cultured in conditional medium (CM) from HBVPs treated with various with concentrations of AS1842856 (0, 0.1, 1 μM), and collected after 8, 12 and 20 h. Scale bars represent 200 μm. n = 4/group. $^{*}P < 0.05$, $^{**}P < 0.01$, $^{***}P < 0.001$. **d, e.** Representative images (d) and wound healing rates (healed area/scratch area%) (e) in the scratch assay showing HUVECs migration under different conditional cultures. Scale bars represent 500 μm. n = 4/group. $^{*}P < 0.05$, $^{**}P < 0.01$, $^{***}P < 0.001$. **f, g.** qPCR analysis of VEGF (f) and ANG-1 (g) mRNA expression in HBVPs treated with various concentrations of AS1842856 for 48 h. n = 4/group. $^{*}P < 0.05$. Data are represented as mean ± SEM and individual points represent independent wells of cultured cells. Statistical comparisons were made using one-way ANOVA with Tukey's *post-hoc* test (b, c and f) or Dunnett's T3 test (e and g).

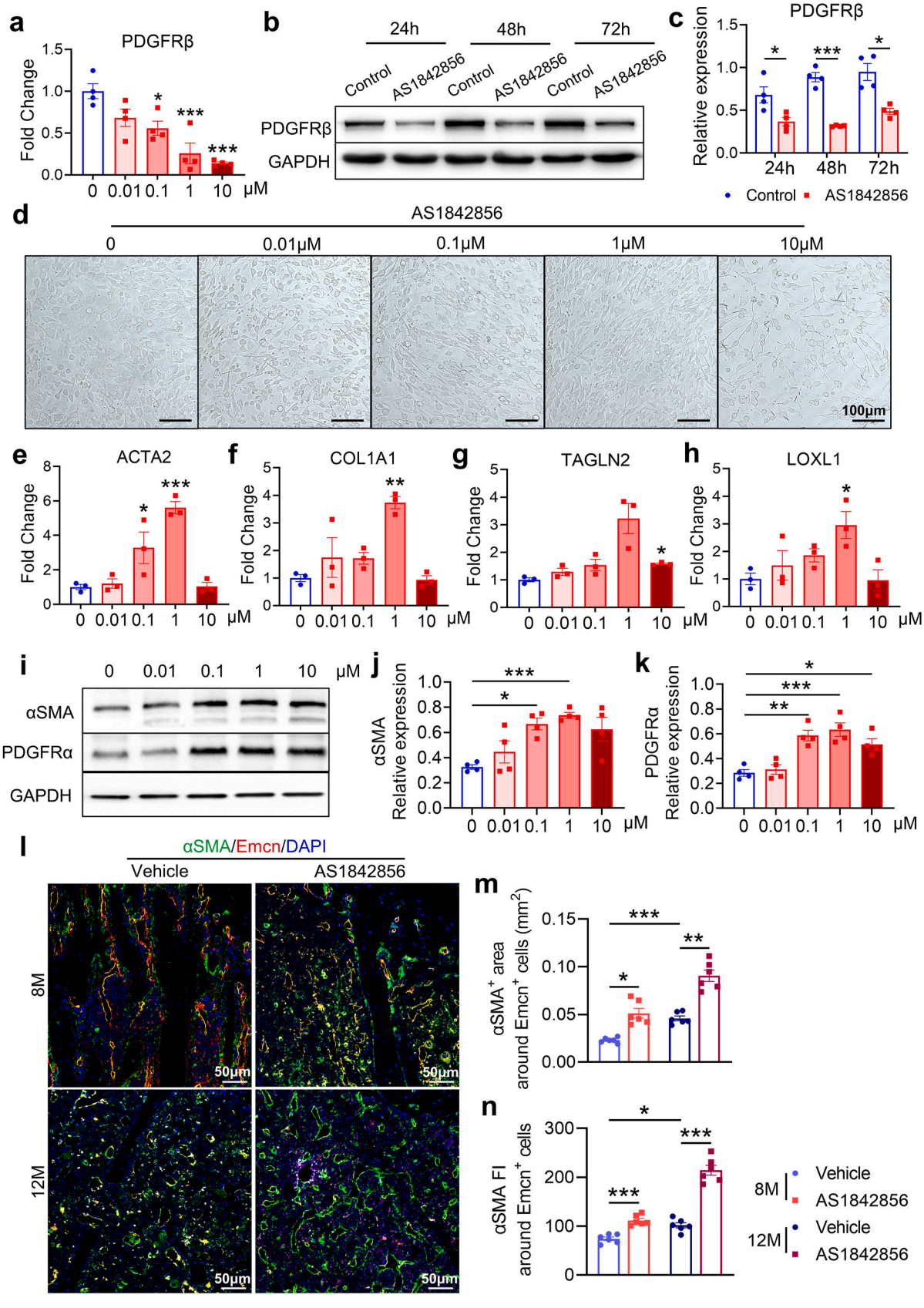

(caption on next page)

Figure 4. Blocking FOXO1 using AS1842856 in pericytes promote their myofibroblastic transformation. a. qPCR analysis of PDGFRβ mRNA expression in HBVPs treated with various concentrations of AS1842856 for 48 h. n = 4/group. $^{*}P < 0.05$, $^{***}P < 0.001$. **b, c.** Western blot analysis (b) and relative levels (c) of PDGFRβ in HBVPs treated with AS1842856 (1 μM) for 24, 48 and 72 h. n = 4/group. $^{*}P < 0.05$, $^{***}P < 0.001$. **d.** Representative images of light field showing fibroblastic morphological changes of HBVPs in response to increasing concentrations of AS1842856 for 48 h. Scale bars represent 100 μm. **e-h.** qPCR analysis of myofibroblast-related gene mRNA levels (ACTA2, COL1A1, TAGLN2 and LOXL1) in HBVPs treated with various concentrations of AS1842856. n = 3/group. $^{*}P < 0.05$, $^{**}P < 0.01$, $^{***}P < 0.001$. **i-k.** Western blotting (i) and quantitative analysis (j and k) of myofibroblastic markers (αSMA and PDGFRα) in HBVPs. n = 4/group. $^{*}P < 0.05$, $^{**}P < 0.01$, $^{***}P < 0.001$. **l.** Representative immunofluorescence images of αSMA (green) and Emcn (red) in the femoral metaphysis of 8- and 12-month-old mice after AS1842856 or vehicle treatment for 2 months. Scale bars represent 50 μm. **m, n.** Quantitative analysis of αSMA fluorescence signal area (m) and intensity (n) around $Emcn^{+}$ vessels. n = 6/group. $^{*}P < 0.05$, $^{**}P < 0.01$, $^{***}P < 0.001$. Data are represented as mean ± SEM and each data point represents an individual cell or animal sample. Statistical comparisons were made using one-way ANOVA with Tukey's *post-hoc* test (equal variances) (a, e, h and k) or Dunnett's T3 test (unequal variances) (c, f, g, j, m and n).

S3a and b). However, Matrigel tube-forming results showed that AS1842856 had little effect on the number of tubule branch points or the length of tubule branches formed by HUVECs (Supplementary Fig. S3c-e). Considering that pericytes are important for maintaining vascular integrity and promoting angiogenesis through their close physical and paracrine contacts with endothelial cells [24,25], we further evaluated the role of pericytic FOXO1 in angiogenesis. Conditional medium (CM) from cultures of HBVPs treated with various concentrations of AS1842856 was collected and subjected to HUVECs culture for Matrigel tube-forming assay. We found that AS1842856-treated CM dose- and time-dependently suppressed tube formation, as revealed by reduced tube length and branch points (Fig. 3a–c). Consistently, scratch assay revealed that migration of HUVECs was suppressed notably by AS1842856-treated CM (Fig. 3d and e). In keeping with the above findings, mRNA expression of VEGF and ANG-1, essential factors for angiogenesis [26], were down-regulated notably by AS1842856 treatment in HBVPs (Fig. 3f and g). The above data indicate that FOXO1 in pericytes plays a critical role in angiogenesis by regulating angiogenesis-associated factors.

3.4. Reduction of FOXO1 activates the pericyte-to-myofibroblast transformation

Given that PDGFRβ, a pericyte marker, is important in regulating the expression of VEGF and ANG-1 [27–29], we detected the effect of AS1842856 on the expression of PDGFRβ in HBVPs. Results showed that AS1842856 treatment significantly down-regulated mRNA and protein expression of PDGFRβ (Fig. 4a–c). Interestingly, with increasing concentrations of AS1842856, HBVPs gradually turned into elongated, shuttle-shaped cells in a "fiber-like" interwoven arrangement (Fig. 4d). Indeed, AS1842856 treatment significantly up-regulated the mRNA expression of fibroblastic marker genes including ACTA2, COL1A1, TAGLN2 and LOXL1 (Fig. 4e–h). Additionally, the protein levels of αSMA and PDGFRα, which are myofibroblastic marker genes, were also notably up-regulated by AS1842856 treatment (Fig. 4i–k). To further determine whether FOXO1 inhibition might promote the pericyte-myofibroblast transformation *in vivo*, we detected the location and expression of αSMA in the bones of mice treated with either vehicle or AS1842856. In 12-month-old mice, αSMA expression around Emcn-labeled vessel-like structures was up-regulated, while $Emcn^{+}$ endothelial cells lost their strip-like morphology in the bone compared with the 8-month-old mice (Fig. 4l–n). AS1842856 treatment further enhanced αSMA expression around these vessel-like structures in bone (Fig. 4l–n). These data therefore support the notion that FOXO1 is essential for maintaining pericyte phenotype and function, thus, loss of FOXO1 may promote the pericyte-to-myofibroblast transformation.

3.5. FOXO1 knockout in pericytes impedes osteogenesis and angiogenesis in mice

Recent study has identified that adiponectin (Adipoq)-positive cells, a unique subpopulation of cells in the bone marrow mesenchymal lineage, exist abundantly as pericytes and stromal cells that form a ubiquitous 3D network inside the marrow cavity [21]. Therefore, *Adipoq-Cre* mice were crossed with $Foxo1^{f/f}$ mice to delete *Foxo1* in $Adipoq^{+}$ cells. We found that *Adipo-Cre/*$Foxo1^{f/f}$ mice were distinguishable from $Foxo1^{f/f}$ control mice by their shorter body and limbs (Supplementary Fig. S4a). We next assessed the effect of *Foxo1* deficiency on mice bone microstructure. Micro-CT analysis revealed a notable loss in trabecular bone and a reduction in cortical bone thickness in *Adipoq-Cre/*$Foxo1^{f/f}$ mice (Fig. 5a, Supplementary Fig. S4b). Quantification confirmed significant decreases in BMD and BV/TV in *Adipoq-Cre/*$Foxo1^{f/f}$ mice (Fig. 5b and c). The reduced bone mass was attributed to decrease in both trabecular number and thickness, coupled with a notable increase in trabecular separation (Fig. 5d–g). Additionally, both cortical bone thickness and cross-sectional area of the femoral diaphysis were significantly reduced in *Adipoq-Cre/*$Foxo1^{f/f}$ mice (Fig. 5a, h and i). The reduction in bone mass was mainly due to impaired bone formation, as indicated by lower serum levels of P1NP in *Adipoq-Cre/*$Foxo1^{f/f}$ mice compared with $Foxo1^{f/f}$ mice (Fig. 5j), while CTX-1 levels remained similar between genotypes (Fig. 5k). Thus, the data support that FOXO1 in $Adipoq^{+}$ cells are functionally important for supporting bone formation.

We next examined whether deficiency of *Foxo1* in $Adipoq^{+}$ cells might impair the type H vessel formation in bone. Double-fluorescence staining for Emcn and CD31 showed that the area of $Emcn^{+}CD31^{+}$ type H vessels was significantly reduced in the bone of *Adipoq-Cre/*$Foxo1^{f/f}$ mice (Fig. 5l and m). Consistent with the effects of pharmacological inhibition of FOXO1 by AS1842856, knocking out *Foxo1* in $Adipoq^{+}$ cells resulted in notably down-regulated expression of PDGFRβ along $Emcn^{+}$ endothelial cells and a significant increase in $αSMA^{+}$ cells in vessel-like structures in bone (Fig. 5n–p). Thus, FOXO1 in $Adipoq^{+}$ pericytic cells is essential for the formation of type H vessels in bone, and loss of FOXO1 may stimulate the transformation of pericytes to myofibroblastic cells, thereby impairing both type H vessel and bone formation.

3.6. Blocking FOXO1 in HBVPs may stimulate the vascular pericytes-to-myofibroblasts transformation by activating mTOR signaling

Accumulating evidence shows that mTOR signaling is involved in myofibroblastic transformation [30]. A recent study has demonstrated the critical role of mTOR signaling in mediating pericyte-myofibroblast transition in choroidal neovascularization [31]. To investigate the possible interplay between FOXO1 and mTOR in regulating vascular pericyte-myofibroblast transition, we examined the expression of FOXO1 and mTOR in HBVPs treated with AS1842856 or rapamycin. Western blot assays revealed that blocking mTOR signaling by rapamycin did not change FOXO1 expression at any of the three time points studied. However, inhibition of FOXO1 using AS1842856 notably stimulated the phosphorylation of mTOR (p-mTOR) at 24 h and 48 h of treatments (Fig. 6a–c). To confirm the regulatory role of FOXO1 in mTOR activation, we used *Foxo1*/pcDNA3.1 for the overexpressed FOXO1 in HBVPs (Supplementary Fig. S5a). Results showed that overexpression of FOXO1 suppressed p-mTOR levels in HBVPs (Fig. 6d and e). These data indicate that down-regulation of FOXO1 may lead to activation of mTOR signaling in pericytes.

To further determine whether blocking FOXO1 may stimulate pericyte-myofibroblast transition by activating mTOR signaling, we

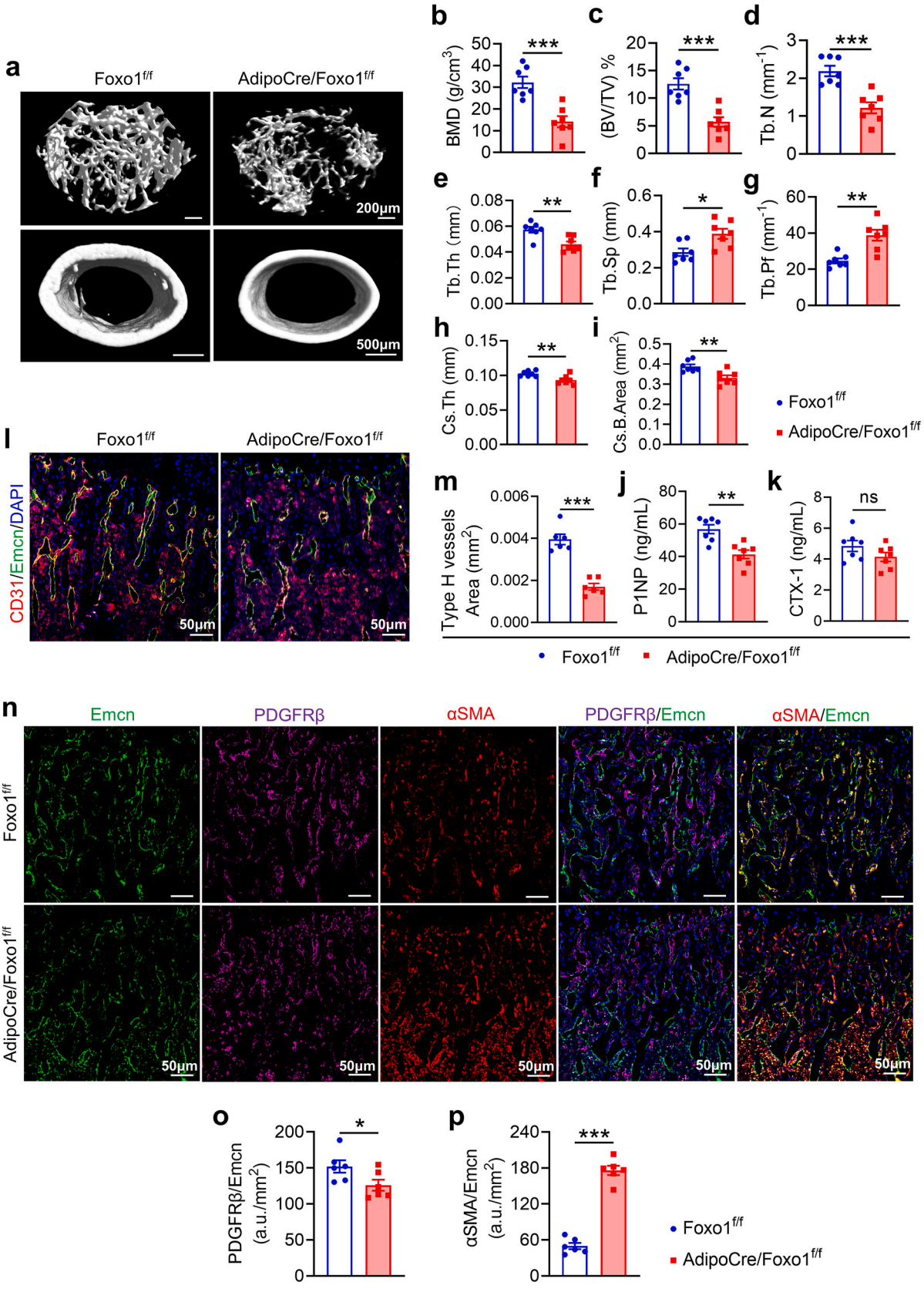

(caption on next page)

Figure 5. Knock-out of *Foxo1* in *Adipoq*$^+$ cells leads to bone loss and degeneration of type H vessels. a. Representative micro-CT images of femoral trabeculae and cortical bone in 4-week-old *Adipo-Cre/Foxo1*$^{f/f}$ and *Foxo1*$^{f/f}$ mice. Scale bars: 200 μm (upper panel), 500 μm (lower panel). **b-i.** Quantitative analysis of three-dimensional structural parameters: bone mineral density (BMD) (b), trabecular bone volume fraction (BV/TV) (c), trabecular number (Tb. N) (d), trabecular thickness (Tb. Th) (e), trabecular separation (Tb. Sp) (f), trabecular pattern factor (Tb. Pf) (g), crossectional thickness (Cs. Th) (h), and crossectional bone area (Cs. B. Area) (i). n = 7/group. *$P < 0.05$, **$P < 0.01$, ***$P < 0.001$. **j, k.** Statistical analysis of serologic bone formation markers P1NP (j) and bone resorption marker CTX-1 (k). n = 7/group. ns, no significance ($P \geq 0.05$), **$P < 0.01$. **l, m.** Representative images (l) and quantitative analysis (m) of immunofluorescence staining for Emcn (green) and CD31 (red) in the femurs of 4-week-old *Adipo-Cre/Foxo1*$^{f/f}$ and *Foxo1*$^{f/f}$ mice. Scale bars represent 50 μm. n = 6/group, ***$P < 0.001$. **n.** Representative immunofluorescence images of perivascular PDGFRβ (purple) and αSMA (red) in the femurs of 4-week-old *Adipo-Cre/Foxo1*$^{f/f}$ and *Foxo1*$^{f/f}$ mice. Scale bars represent 50 μm. **o, p.** Relative fluorescence intensity (a. u.) of PDGFRβ and αSMA per Emcn$^+$ area in the field of view. n = 6/group. *$P < 0.05$, ***$P < 0.001$. Data are represented as mean ± SEM. Each data point represents one animal. Statistical comparisons were made using Student's *t*-test.

treated HBVPs with AS1842856, rapamycin, or a combination of both. Based on the morphological characteristics of HBVPs, while rapamycin treatment alone had no effect on HBVPs morphology, it blocked the effect of AS1842856-induced spindle-like morphology in HBVPs (Supplementary Fig. S5b). Western blot analysis confirmed that rapamycin treatment blocked αSMA expression induced by AS1842856 and suppressed PDGFRα expression (Supplementary Fig. 5c and 5dSupplementary Fig. S5c and d). Given that FOXO proteins are a family of transcription factors with four members in mammals, including FOXO1, FOXO3a, FOXO4, and FOXO6 [32,33], we evaluated whether AS1842856 might have non-specific effect on the other family members. Results showed that AS1842856 had no effect on the mRNA expression of other FOXO members (Supplementary Fig. S5e-g). Thus, these data indicate that AS1842856 activates mTOR signaling specifically by blocking FOXO1, thereby stimulates pericyte-myofibroblast transition.

To further specify the role of FOXO1 in pericyte-myofibroblast transition, we designed siRNAs against *Foxo1* and selected the siRNA#2 fragment with the highest knockdown efficiency for subsequent experiments (Supplementary Fig. S6a and b). This siRNA fragment had no effects on the mRNA expression of *Foxo3a*, *Foxo4*, and *Foxo6* in HBVPs (Supplementary Fig. S6c). Immunofluorescence staining data showed that *Foxo1* knockdown promoted αSMA expression and the nucleus location of p-mTOR in HBVPs, while rapamycin blocked the above effects (Fig. 6f–h). Consistently, western blot analysis confirmed that rapamycin treatment blocked the up-regulation of αSMA expression induced by *Foxo1*-siRNA and concurrently suppressed PDGFRα expression (Fig. 6i–k). Furthermore, overexpression of FOXO1 significantly suppressed the expression of αSMA and PDGFRα, similar to the effects observed with rapamycin (Fig. 6l–n). Thus, these suggest that the upregulation of mTOR signaling contributes to the pericytes-to-myofibroblasts transformation in the context of FOXO1 deficiency.

3.7. FOXO1 suppresses the vascular pericyte-to-myofibroblast transformation by inhibiting mTOR signaling in murine bone

To confirm the regulatory role of FOXO1 in mTOR signaling in vascular pericytes *in vivo*, we detected p-mTOR levels in vascular pericytes of *Adipoq-Cre/Foxo1*$^{f/f}$ mice by immunofluorescence staining. Results showed a notable up-regulation of PDGFRα expression in metaphyseal bone area (Fig. 7a and b), and a significant increase in p-mTOR expression in PDGFRα$^+$ cells of *Adipoq-Cre/Foxo1*$^{f/f}$ mice compared with *Foxo1*$^{f/f}$ mice (Fig. 7a and c). In addition, 12-month-old mice displayed higher levels of PDGFRα and p-mTOR in the metaphyseal bone area compared with 8-month-old mice (Fig. 7d–f). Moreover, AS1842856 treatment resulted in a significant increase in both PDGFRα and p-mTOR levels, with a pronounced increase in p-mTOR level in PDGFRα$^+$ cells (Fig. 7d–g). These data suggest that FOXO1 deficiency activates mTOR signaling in PDGFRα$^+$ cells.

To evaluate the impact of mTOR on age-associated degeneration of type H vessels, we administered rapamycin to middle-aged mice. The results showed that rapamycin significantly increased the number of type H vessels in the metaphyseal bone of middle-aged mice (Fig. 8a and b). Furthermore, rapamycin treatment led to a significant increase in PDGFRβ expression, a pericytes marker, and a dramatic decrease in αSMA expression, a myofibroblast marker (Fig. 8c–e). H&E staining and quantification showed that rapamycin significantly elevated the number of osteoblasts in the metaphyseal bone of middle-aged mice (Supplementary Fig. S7a and b). In consistent, micro-CT analysis revealed improvements in both trabecular and cortical bone mass in these mice (Fig. 8f). Quantitative analysis demonstrated that rapamycin treatment significantly increased BMD and BV/TV (Fig. 8g and h), primarily due to increased Tb.Th and decreased Tb.Sp, with no significant change in Tb. N (Fig. 8i–k). Although cortical thickness remained unchanged, the cortical bone area was improved by rapamycin treatment (Fig. 8l and m). Serum biochemistry assays showed that rapamycin significantly increased circulating P1NP levels while decreased CTX-1 levels in middle-aged mice (Fig. 8n and o). Together, these results indicate that FOXO1 is an essential factor for maintaining the phenotype of vascular pericyte by suppressing mTOR signaling.

4. Discussion

FOXO1, an important "protective gene" [34], plays a critical role in preventing cellular and organismal aging [35]. However, its function in bone degeneration is still unclear. In this study, we demonstrated that the transformation of pericytes into myofibroblast, induced by FOXO1 deficiency in pericytes, is a core mechanism underlying age-associated reduction in type H vessels and trabecular bone loss. Furthermore, we uncovered a new mechanism by which FOXO1 might preserve the phenotype of pericytes by suppressing TORC1 signaling. Our findings of the roles of FOXO1 in regulating bone metabolism have significantly extended upon previous studies that primarily focused on osteogenic activity and proliferation of osteoprogenitors [18,19,36].

Our study highlights the fact that the function of FOXO1 in bone metabolism is highly dependent on cellular context. Previous evidence showed that specific deletion of FOXO1 in mature osteoblasts using *Col1a1-Cre* or broad deletion of *Foxo1, -3,* and *-4* in early progenitors using *Mx1-Cre* caused loss of bone mass [37,38]. Conversely, deletion of *Foxo1, -3*, and *-4* in committed osteoblasts using *Osterix-Cre* led to increased bone mass [18]. Recent evidence showed that knockout of *Foxo1* using *Bglap-Cre* led to bone loss in young mice but alleviated age-associated bone loss in older mice [19]. However, it is somehow unexpected that deletion of *Foxo1* using *Col2-Cre (ERT)* had no effect on bone mass in 10-month-old mice. It is important to note that *Col2*-targeted cells contribute not only to chondrocytes and perichondrial cells in growth cartilage but also a majority of osteoblast and mesenchymal progenitors in metaphyseal bone [21,22]. Considering the distinct functions of FOXO1 in osteoblastic lineage cells at different stages [19,37,38], these discrepant findings might be attributed to multiple cell types within the *Col2*-linage, including mesenchymal progenitors, osteoblasts, osteocytes, and adipocytes in adult and old mice [21,22,39]. Furthermore, our observation that pharmacological inhibition of FOXO1 leads to significant bone loss in both adult and middle-aged mice suggests that FOXO1 in non-*Col2*$^+$ bone marrow cells may play a critical role in modulating bone metabolism.

Our study has revealed a critical role of FOXO1 in maintaining type H vessels in aging bone. Although it is well recognized that type H vessels in bone are fundamentally important for bone modeling and remodeling [23], and age-related bone loss is associated with the decline of type H vessels and the concomitant reduction in osteoprogenitors [8,10,40],

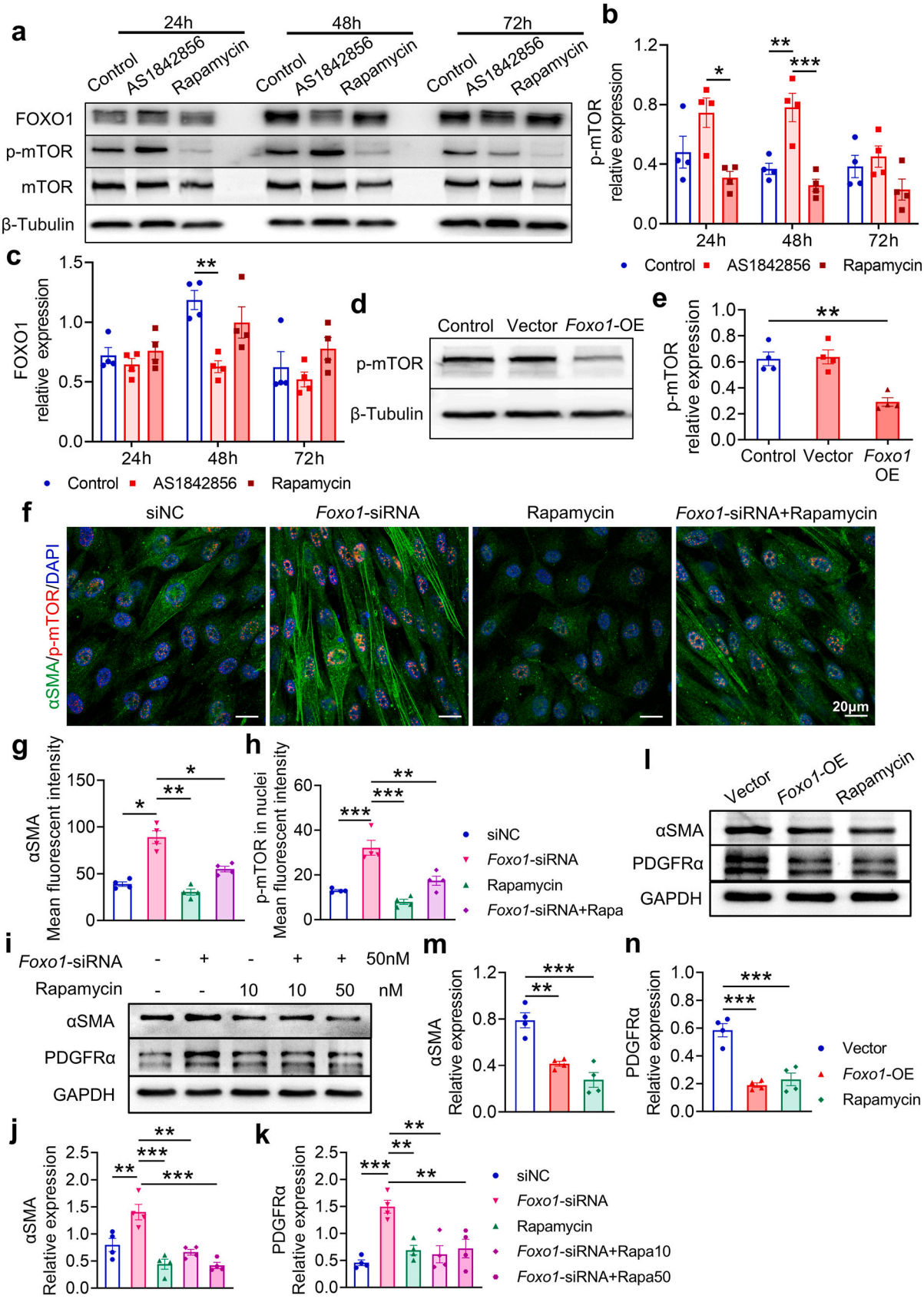

(caption on next page)

Figure 6. FOXO1 maintains the phenotype of pericytes by suppressing mTOR signaling. a-c. Western blotting (a) and quantitative analysis of p-mTOR (b) and FOXO1 (c) in HBVPs after 24, 48, and 72 h of treatment with AS1842856 (1 μM) or Rapamycin (10 nM). n = 4/group. $^{*}P < 0.05$, $^{**}P < 0.01$, $^{***}P < 0.001$. **d, e.** Western blotting (d) and quantitative analysis (e) of p-mTOR in HBVPs after transfection with *Foxo1*/pcDNA3.1 or pcDNA3.1. n = 4/group. $^{**}P < 0.01$. **f-h.** Representative cell immunofluorescence staining and quantification of the mean fluorescence intensity for αSMA (green) and nuclear-localized p-mTOR (red) in HBVPs after indicated treatments. Nuclei were stained with DAPI. Scale bars represent 20 μm. n = 4/group. $^{*}P < 0.05$, $^{**}P < 0.01$, $^{***}P < 0.001$. **i-k.** Western blotting (i) and quantitative analysis (j and k) of protein levels of αSMA and PDGFRα in HBVPs after indicated treatment for 48 h. n = 4/group. $^{**}P < 0.01$, $^{***}P < 0.001$. **l-n.** Western blotting (l) and quantitative analysis of changes on αSMA (m) and PDGFRα (n) in HBVPs after 48 h of transfection with plasmids. n = 4/group. $^{**}P < 0.01$, $^{***}P < 0.001$. Data are displayed as mean ± SEM. Each data point represents an independent cell sample. Statistical comparisons were made using one-way ANOVA with Tukey's *post-hoc* test (equal variances) (b, c, h, j, k, m and n) or Dunnett's T3 test (unequal variances) (e and g).

the molecular mechanisms driving the age-associated degeneration of type H vessels are poorly understood. Earlier studies have indicated that FOXO1 is an essential regulator of vascular growth. For instance, either full or epithelial-specific knockout of *Foxo1* induces embryonic lethality due to incomplete vascular development [41,42]. Consistent with this notion, here we show that pharmacological inhibition of FOXO1 decreases the number of type H vessels in adult mice and exacerbates this reduction in middle-aged mice, correlating with severe bone loss. Our study suggests that FOXO1 may be critical to the stability of type H vessels, thereby maintaining the bone mass. In consistent with a recent study indicating decreased FOXO1 mRNA expression in the bone with aging [19], we observed a decreased protein level of FOXO1 in the bone of aged mice. Interestingly, while pharmacological inhibition of FOXO1 using AS1842856 did not directly affect tubule formation in HUVECs, conditional medium from AS1842856-treated pericytes impaired tubule formation in HUVECs. Additionally, our study found decreased FOXO1 expression in PDGFRβ^{+} pericytes surrounding type H vessels. Furthermore, conditional knockout of *Foxo1* in *Adipoq*$^{+}$ cells led to reduced type H vessels and a considerable reduction in bone mass, suggesting that FOXO1 reduction in pericytes may mediate the degeneration of type H vessels in aged mice.

It is important to note that mice harboring Adipoq-Cre can also target the floxed *Foxo1* in white and brown adipose tissue, in addition to bone marrow [43]. While specific silencing of *Foxo1* in *Adipoq*$^{+}$ cells promote browning of adipose tissue and activates metabolic pathways [44,45], it has been shown that fat transplantation does not rescue distorted bone marrow vasculature and bone loss after ablating *Adipoq*$^{+}$ cells [21]. Thus, *Foxo1* deficiency in peripheral fat tissues may not be involved in the changes in bone vessels and bone mass. Additionally, *Adipoq*$^{+}$ cells are as abundant as both pericytes and stromal cells in the bone marrow [21]. Besides modulating osteogenesis and osteoclastogenesis [46–50], bone marrow *Adipoq*$^{+}$ cells have recently been revealed to play functional role in regulating type H vessel formation by secreting osteopontin [47]. Therefore, the potential role of FOXO1 in bone marrow *Adipoq*$^{+}$ stromal cells regarding the formation of type H vessels *in vivo* cannot be disregarded. Despite this, our present data demonstrate that the reduction of FOXO1 in pericytes is at least one of the important mechanisms underlying the degeneration of type H vessels with aging.

Our findings have provided a new understanding of the mechanism by which FOXO1 maintains the pericytes phenotype in type H vessels by suppressing mTOR signaling. As essential components of the microvascular vessel wall, pericytes are one of the main sources of VEGFA and ANG-1, which are critical factors for vessel formation and stabilization [51–53]. Our findings have identified FOXO1 as a regulatory factor for the expression of VEGF and ANG-1 in pericytes, with a critical role of in endothelial tubule formation and angeiogenesis. Recent studies have demonstrated an age-dependent decline in vascular density and a loss of pericytes, accompanied by a transformation from pericytes to fibroblasts, contributing to the loss of pericytes in tissues [54]. Likewise, our work shows a reduction in PDGFRβ^{+} pericytes and an increase in fibroblasts along the of vessel walls in the metaphyseal bone of aged-mice or mice treated with FOXO1 inhibitors. Additionally, our finding further identifies FOXO1 as a key upstream inhibitor of mTORC1, both *in vivo* and *in vitro*, thereby supporting the phenotype and function of pericytes. Therefore, down-regulation of FOXO1 in pericytes is at least one of the underlying mechanisms whereby type H vessels degenerate upon transformation of pericytes-to-fibroblasts.

mTORC is a critical signaling molecule implicated in tissue degeneration and metabolism-related pathology [30]. A collection of rapamycin derivatives, the mTORC inhibitors, has been approved for anticancer treatment in clinic [55,56]. In addition, growing clinical and laboratory evidence has highlighted rapamycin derivatives as promising treatments for age-associated neurodegenerative diseases [57,58]. However, the exact role of mTORC in bone metabolism varies under different conditions. Inhibition of mTOR signaling using rapamycin or genetic inactivation of mTORC1 by deleting Raptor in pre-osteoblasts has been revealed to induce bone loss in mice [59,60]. Conversely, an increased level of mTOR can suppress both bone formation and angiogenesis in osteoporotic animal models, and osteocyte-specific down--regulation or pharmacological inhibition of mTORC signaling has been shown to increase bone mass [61,62]. The conflicting effects of blocking mTORC1 on bone metabolism may be due to critical roles of mTORC1 signaling in various cell types in bone tissue. Here, our study provides strong evidence that long-term rapamycin treatment at a low dose ameliorate age-associated degeneration in bone. A recent study has implicated mTOR signaling in the pericyte-myofibroblast transition in subretinal fibrosis in age-related macular degeneration [31]. Our studies extend this finding that mTORC1 signaling mediates the pericyte-myofibroblast transition in type H vessels in aged bone. It will be interesting to further investigate how FOXO1 suppresses mTOR signaling in pericytes.

Taken together, our findings shed light on the role of FOXO1 in regulating both the phenotype and function of pericytes, thereby promoting the formation of type H vessels. Moreover, we provide novel insights into the mechanisms by which FOXO1 preserves phenotype of pericytes by suppressing mTOR signaling and retains its function in angiogenesis by regulating the expression of VEGF and ANG-1.

Ethics statement

All animal experiments were performed according to the protocols approved by the Institutional Animal Care and Use Committee (IACUC) (NFYY-2020-0933) at Southern Medical University Nanfang Hospital, and all procedures were carried out following IACUC guidelines.

Authorship

All persons who meet authorship criteria are listed as authors, and all authors certify that they have participated sufficiently in the work to take public responsibility for the content, including participation in the concept, design, analysis, writing, or revision of the manuscript. Each author certifies that this material or part thereof has not been published in another journal, that it is not currently submitted elsewhere, and that it will not be submitted elsewhere until a final decision regarding publication of the manuscript in Journal of Orthopaedic Translation has been made.

Indicate the specific contributions made by each author (list the authors' initials followed by their surnames, e.g., Y.L. Cheung). The name of each author must appear at least once in each of the three categories below.

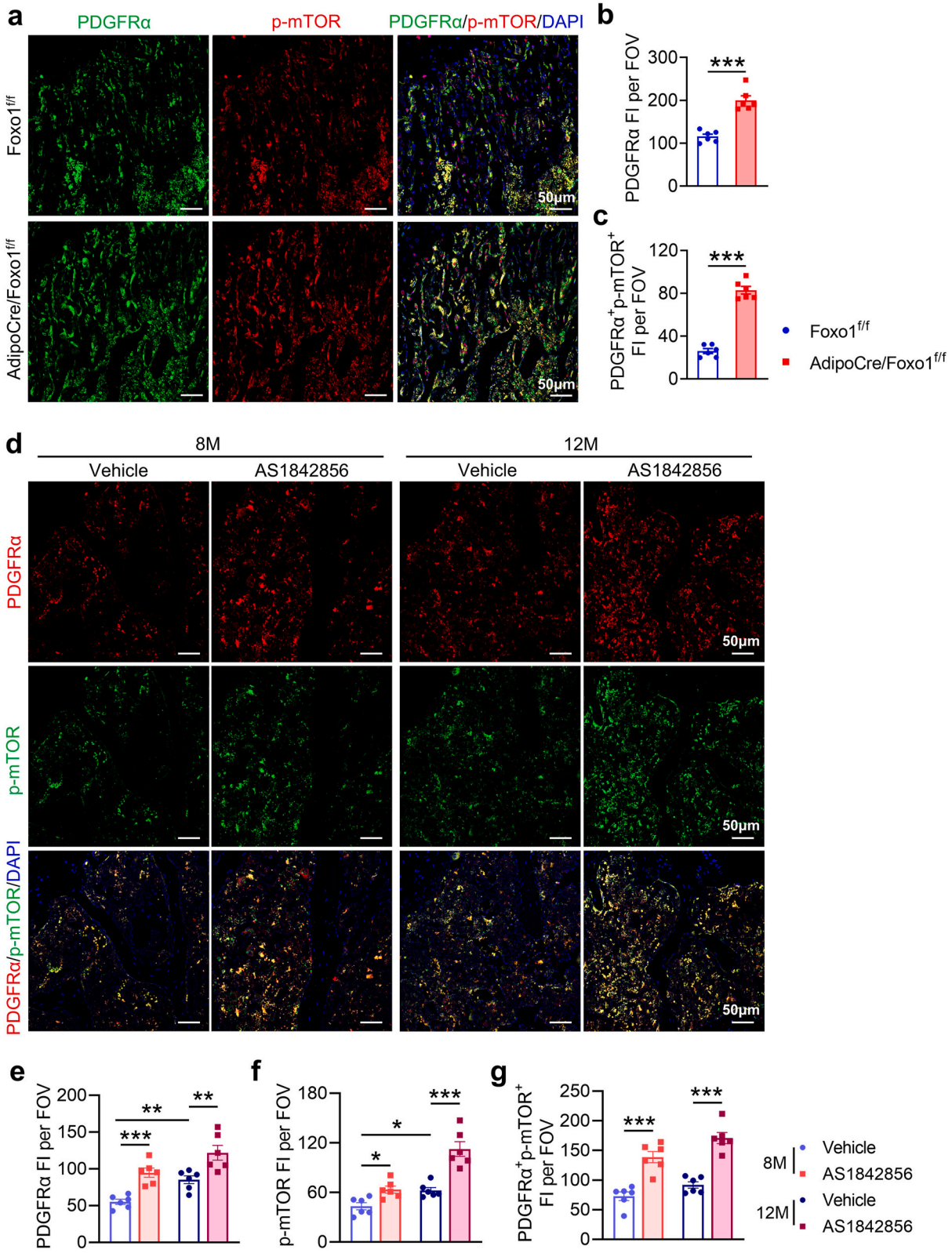

Figure 7. FOXO1 in PDGFRα$^+$ pericytes maintains type H vessels by inhibiting mTOR signaling in mice bone. a. Representative immunofluorescence images of PDGFRα (green) and p-mTOR (red) in the femoral metaphysis of 4-week-old *Adipo-Cre/Foxo1$^{f/f}$* and *Foxo1$^{f/f}$* mice. Nuclei were stained DAPI. Scale bars represent 50 μm. **b, c.** Quantitative analysis of PDGFRα$^+$ fluorescence intensity (b) and PDGFRα$^+$ p-mTOR$^+$ colocalization fluorescence intensity (c). n = 6/group. ***$P <$ 0.001. **d.** Representative immunofluorescence images of PDGFRα (red) and p-mTOR (green) in 8- and 12-month-old mice treated with AS1842856. Nuclei were stained DAPI. Scale bars represent 50 μm. **e-g.** Quantitative analysis of PDGFRα$^+$ (e), phosphorylated mTOR$^+$ (f), and their colocalization (g) fluorescence signal intensities. n = 6/group. *$P < 0.05$, **$P < 0.01$, ***$P < 0.001$. Data are represented as mean ± SEM. Each data point represents one animal. Statistical comparisons were made using Student's *t*-test (equal variances) (b and c) or one-way ANOVA with Tukey's *post-hoc* test (equal variances) (e, f and g).

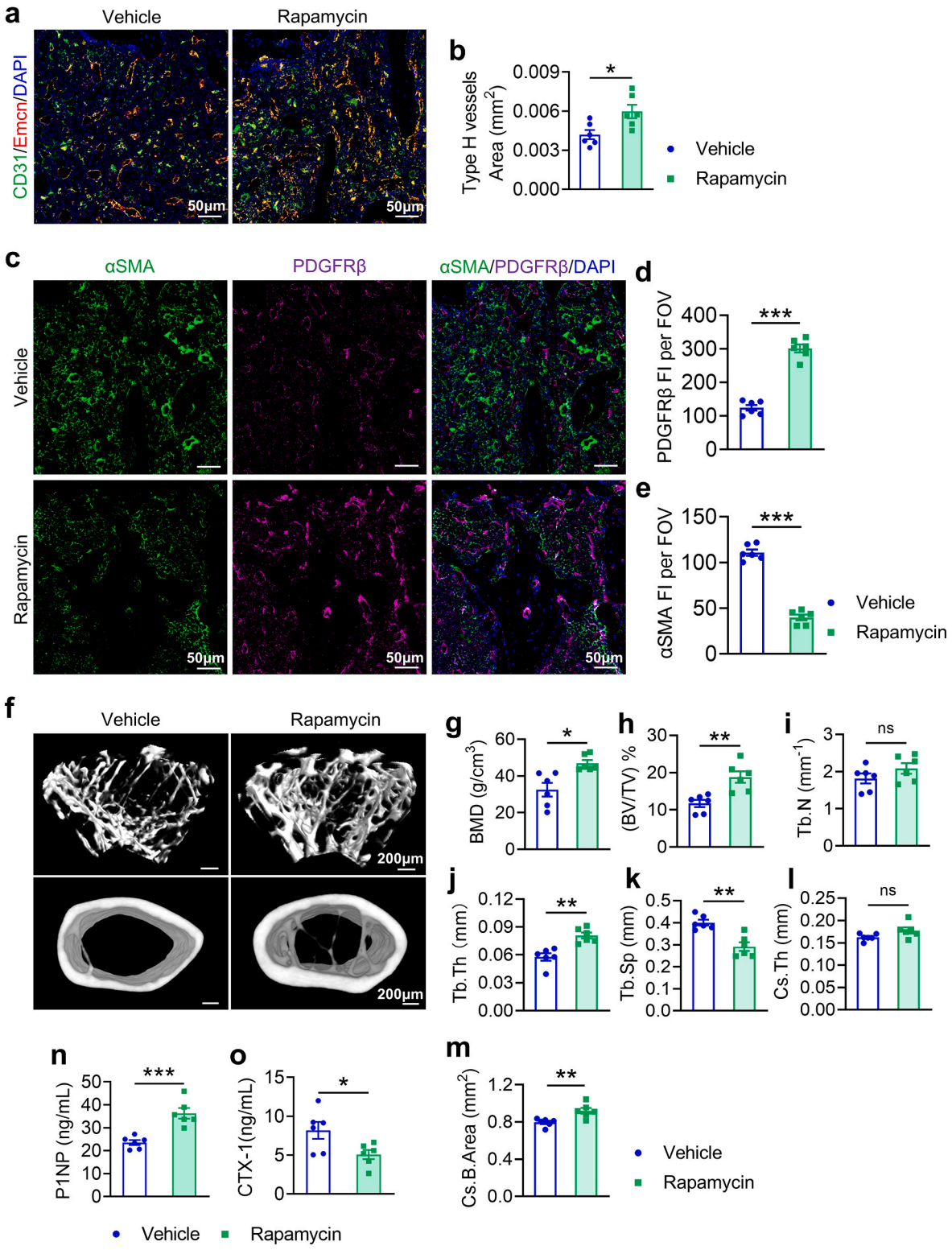

Figure 8. Rapamycin diminishes pericyte-myofibroblast transformation and ameliorates type H vessels degeneration and bone loss in mice. a, b. Representative images (a) and quantitative analysis (b) of the immunofluorescence staining of type H vessels (CD31 and Emcn) in the femoral epiphysis of 12-month-old mice treated with rapamycin (2 mg/kg) for 4 weeks. Nuclei were stained with DAPI. Scale bars represent 50 μm. n = 6/group. $^{*}P < 0.05$. **c-e.** Representative images (c) and quantitative analysis (d and e) of the immunofluorescence staining of PDGFRβ^{+} (purple) and αSMA^{+} (green) in the femoral epiphysis of mice. Nuclei were stained with DAPI. Scale bars represent 50 μm. n = 6/group. $^{***}P < 0.001$. **f.** Representative micro-CT reconstructions of trabecular and cortical bone in the femoral epiphysis of mice. Scale bars represent 200 μm. **g-m.** Quantitative analysis of micro-CT structural parameters: bone mineral density (BMD) (g), trabecular bone volume fraction (BV/TV) (h), trabecular number (Tb. N) (i), trabecular thickness (Tb. Th) (j), trabecular separation (Tb. Sp) (k), crossectional thickness (Cs. Th) (l), and cross-sectional bone area (Cs. B. Area) (m). n = 6/group. ns, no significance ($P \geq 0.05$), $^{*}P < 0.05$, $^{**}P < 0.01$. **n, o.** Quantitative ELISA analysis of serum P1NP (n) and CTX-1 (o). n = 6/group. $^{*}P < 0.05$, $^{***}P < 0.001$. Data are represented as mean ± SEM. Each data point represents one animal. Statistical comparisons were made using Student's *t* test (b, d, e, h, i, j, k, l, m, n and o) or Mann–Whitney U test (unequal variances) (g).

Section I

The authors whose names are listed immediately below certify that they have NO affiliations with or involvement in any organization or entity with any financial interest (such as honoraria; educational grants; participation in speakers' bureaus; membership, employment, consultancies, stock ownership, or other equity interest; and expert testimony or patent-licensing arrangements), or non-financial interest (such as personal or professional relationships, affiliations, knowledge or beliefs) in the subject matter or materials discussed in this manuscript.

Authors: C.Y. Cheng, M.Y. Deng, C.B. Cheng, H.T. Wu, Y.T. Wang, M. C. Lu, Z.L. Yao, K.Q. Li, X.R. Zhang, B. Yu.

Section II

The authors whose names are listed immediately below report the following details of affiliation or involvement in an organization or entity with a financial or non-financial interest in the subject matter or materials discussed in this manuscript. Please specify the nature of the conflict on a separate sheet of paper if the space below is inadequate.

None

CRediT authorship contribution statement

Conceptualization, **X.R. Zhang, B. Yu** and **C.Y. Cheng**; Methodology, mouse experiments, **C.Y. Cheng, M.Y. Deng** and **H.T. Wu**; In vitro experiments, **C.Y. Cheng, M.Y. Deng** and **C.B. Cheng**; Collection of samples from individuals and analysis, **Y.T. Wang, M.C. Lu** and **C.B. Cheng**; Formal analysis, **K.Q. Li** and **Z.L. Yao**; Writing–Original Draf, **C. Y. Cheng** and **M.Y. Deng**; Writing–Review & Editing, **X.R. Zhang** and **C.Y. Cheng**; Funding Acquisition, **B. Yu, X.R. Zhang** and **K.Q. Li**; Project Administration and Supervision, **X.R. Zhang** and **B. Yu**.

Declaration of competing interest

The authors declare no conflict of interest that could have appeared to influence the work reported in this paper.

Acknowledgements

We gratefully acknowledge all individuals who participated in the study. We thank Prof. Liang Ping for English proofreading of the manuscript. This study was supported by funding from The Major Program of National Natural Science Foundation of China (81830079, to B. Y.); National Natural Science Foundation of China (82072459, to X.Z.); and Science and Technology Projects of Guangzhou (202201011339).

Appendix A. Supplementary data

Supplementary data to this article can be found online at https://doi.org/10.1016/j.jot.2024.08.010.

References

[1] Clynes MA, Harvey NC, Curtis EM, Fuggle NR, Dennison EM, Cooper C. The epidemiology of osteoporosis. Br Med Bull 2020;133(1):105–17. https://doi.org/10.1093/bmb/ldaa005.
[2] Wang L, Yu W, Yin X, Cui L, Tang S, Jiang N, et al. Prevalence of osteoporosis and fracture in China: the China osteoporosis prevalence study. JAMA Netw Open 2021;4(8):e2121106. https://doi.org/10.1001/jamanetworkopen.2021.21106.
[3] LeBoff MS, Greenspan SL, Insogna KL, Lewiecki EM, Saag KG, Singer AJ, et al. The clinician's guide to prevention and treatment of osteoporosis. Osteoporos Int 2022;33(10):2049–102. https://doi.org/10.1007/s00198-021-05900-y.
[4] Liang B, Burley G, Lin S, Shi YC. Osteoporosis pathogenesis and treatment: existing and emerging avenues. Cell Mol Biol Lett 2022;27(1):72. https://doi.org/10.1186/s11658-022-00371-3.
[5] Reid IR, Billington EO. Drug therapy for osteoporosis in older adults. Lancet 2022;399(10329):1080–92. https://doi.org/10.1016/s0140-6736(21)02646-5.
[6] Fink HA, MacDonald R, Forte ML, Rosebush CE, Ensrud KE, Schousboe JT, et al. Long-term drug therapy and drug discontinuations and holidays for osteoporosis fracture prevention: a systematic review. Ann Intern Med 2019;171(1):37–50. https://doi.org/10.7326/m19-0533.
[7] Saag KG, Petersen J, Brandi ML, Karaplis AC, Lorentzon M, Thomas T, et al. Romosozumab or alendronate for fracture prevention in women with osteoporosis. N Engl J Med 2017;377(15):1417–27. https://doi.org/10.1056/NEJMoa1708322.
[8] Kusumbe AP, Ramasamy SK, Adams RH. Coupling of angiogenesis and osteogenesis by a specific vessel subtype in bone. Nature 2014;507(7492):323–8. https://doi.org/10.1038/nature13145.
[9] Itkin T, Gur-Cohen S, Spencer JA, Schajnovitz A, Ramasamy SK, Kusumbe AP, et al. Distinct bone marrow blood vessels differentially regulate haematopoiesis. Nature 2016;532(7599):323–8. https://doi.org/10.1038/nature17624.
[10] Wang L, Zhou F, Zhang P, Wang H, Qu Z, Jia P, et al. Human type H vessels are a sensitive biomarker of bone mass. Cell Death Dis 2017;8(5):e2760. https://doi.org/10.1038/cddis.2017.36.
[11] Yang M, Li CJ, Sun X, Guo Q, Xiao Y, Su T, et al. MiR-497~195 cluster regulates angiogenesis during coupling with osteogenesis by maintaining endothelial Notch and HIF-1α activity. Nat Commun 2017;8:16003. https://doi.org/10.1038/ncomms16003.
[12] Berthiaume AA, Schmid F, Stamenkovic S, Coelho-Santos V, Nielson CD, Weber B, et al. Pericyte remodeling is deficient in the aged brain and contributes to impaired capillary flow and structure. Nat Commun 2022;13(1):5912. https://doi.org/10.1038/s41467-022-33464-w.
[13] Watson AN, Berthiaume AA, Faino AV, McDowell KP, Bhat NR, Hartmann DA, et al. Mild pericyte deficiency is associated with aberrant brain microvascular flow in aged PDGFRβ(+/-) mice. J Cerebr Blood Flow Metabol 2020;40(12):2387–400. https://doi.org/10.1177/0271678x19900543.
[14] Stobart JL, Erlebach E, Glück C, Huang SF, Barrett MJ, Li M, et al. Altered hemodynamics and vascular reactivity in a mouse model with severe pericyte deficiency. J Cerebr Blood Flow Metabol 2023;43(5):763–77. https://doi.org/10.1177/0271678x221147366.
[15] Zhu S, Chen M, Ying Y, Wu Q, Huang Z, Ni W, et al. Versatile subtypes of pericytes and their roles in spinal cord injury repair, bone development and repair. Bone Res 2022;10(1):30. https://doi.org/10.1038/s41413-022-00203-2.
[16] Accili D, Arden KC. FoxOs at the crossroads of cellular metabolism, differentiation, and transformation. Cell 2004;117(4):421–6. https://doi.org/10.1016/s0092-8674(04)00452-0.
[17] Wilhelm K, Happel K, Eelen G, Schoors S, Oellerich MF, Lim R, et al. FOXO1 couples metabolic activity and growth state in the vascular endothelium. Nature 2016;529(7585):216–20. https://doi.org/10.1038/nature16498.
[18] Iyer S, Ambrogini E, Bartell SM, Han L, Roberson PK, de Cabo R, et al. FOXOs attenuate bone formation by suppressing Wnt signaling. J Clin Invest 2013;123(8):3409–19. https://doi.org/10.1172/jci68049.
[19] Xiong Y, Zhang Y, Zhou F, Liu Y, Yi Z, Gong P, et al. FOXO1 differentially regulates bone formation in young and aged mice. Cell Signal 2022;99:110438. https://doi.org/10.1016/j.cellsig.2022.110438.
[20] Andrade J, Shi C, Costa ASH, Choi J, Kim J, Doddaballapur A, et al. Control of endothelial quiescence by FOXO-regulated metabolites. Nat Cell Biol 2021;23(4):413–23. https://doi.org/10.1038/s41556-021-00637-6.
[21] Zhong L, Yao L, Tower RJ, Wei Y, Miao Z, Park J, et al. Single cell transcriptomics identifies a unique adipose lineage cell population that regulates bone marrow environment. Elife 2020;9. https://doi.org/10.7554/eLife.54695.
[22] O W O N, Nagasawa T, Kronenberg HM. A subset of chondrogenic cells provides early mesenchymal progenitors in growing bones. Nat Cell Biol 2014;16(12):1157–67. https://doi.org/10.1038/ncb3067.
[23] Peng Y, Wu S, Li Y, Crane JL. Type H blood vessels in bone modeling and remodeling. Theranostics 2020;10(1):426–36. https://doi.org/10.7150/thno.34126.
[24] Figueiredo AM, Villacampa P, Diéguez-Hurtado R, José Lozano J, Kobialka P, Cortazar AR, et al. Phosphoinositide 3-kinase-regulated pericyte maturation governs vascular remodeling. Circulation 2020;142(7):688–704. https://doi.org/10.1161/circulationaha.119.042354.
[25] Teichert M, Milde L, Holm A, Stanicek L, Gengenbacher N, Savant S, et al. Pericyte-expressed Tie2 controls angiogenesis and vessel maturation. Nat Commun 2017;8:16106. https://doi.org/10.1038/ncomms16106.
[26] Chidiac R, Zhang Y, Tessier S, Faubert D, Delisle C, Gratton JP. Comparative phosphoproteomics analysis of VEGF and angiopoietin-1 signaling reveals ZO-1 as a critical regulator of endothelial cell proliferation. Mol Cell Proteomics 2016;15(5):1511–25. https://doi.org/10.1074/mcp.M115.053298.
[27] Andrae J, Gallini R, Betsholtz C. Role of platelet-derived growth factors in physiology and medicine. Genes Dev 2008;22(10):1276–312. https://doi.org/10.1101/gad.1653708.
[28] Kim I, Ryu YS, Kwak HJ, Ahn SY, Oh JL, Yancopoulos GD, et al. EphB ligand, ephrinB2, suppresses the VEGF- and angiopoietin 1-induced Ras/mitogen-activated protein kinase pathway in venous endothelial cells. Faseb J 2002;16(9):1126–8. https://doi.org/10.1096/fj.01-0805fje.
[29] Tarnawski AS, Ahluwalia A. The critical role of growth factors in gastric ulcer healing: the cellular and molecular mechanisms and potential clinical implications. Cells 2021;10(8). https://doi.org/10.3390/cells10081964.
[30] Liu GY, Sabatini DM. mTOR at the nexus of nutrition, growth, ageing and disease. Nat Rev Mol Cell Biol 2020;21(4):183–203. https://doi.org/10.1038/s41580-019-0199-y.
[31] Zhao Z, Zhang Y, Zhang C, Zhang J, Luo X, Qiu Q, et al. TGF-β promotes pericyte-myofibroblast transition in subretinal fibrosis through the Smad2/3 and Akt/

mTOR pathways. Exp Mol Med 2022;54(5):673–84. https://doi.org/10.1038/s12276-022-00778-0.
[32] Gui T, Burgering BMT. FOXOs: masters of the equilibrium. FEBS J 2022;289(24):7918–39. https://doi.org/10.1111/febs.16221.
[33] Ma X, Su P, Yin C, Lin X, Wang X, Gao Y, et al. The roles of FoxO transcription factors in regulation of bone cells function. Int J Mol Sci 2020;21(3). https://doi.org/10.3390/ijms21030692.
[34] Martins R, Lithgow GJ, Link W. Long live FOXO: unraveling the role of FOXO proteins in aging and longevity. Aging Cell 2016;15(2):196–207. https://doi.org/10.1111/acel.12427.
[35] Matsuzaki T, Alvarez-Garcia O, Mokuda S, Nagira K, Olmer M, Gamini R, et al. FoxO transcription factors modulate autophagy and proteoglycan 4 in cartilage homeostasis and osteoarthritis. Sci Transl Med 2018;10(428). https://doi.org/10.1126/scitranslmed.aan0746.
[36] Wang Z, Zhou F, Feng X, Li H, Duan C, Wu Y, et al. FoxO1/NLRP3 inflammasome promotes age-related alveolar bone resorption. J Dent Res 2023;102(8):919–28. https://doi.org/10.1177/00220345231164104.
[37] Ambrogini E, Almeida M, Martin-Millan M, Paik JH, Depinho RA, Han L, et al. FoxO-mediated defense against oxidative stress in osteoblasts is indispensable for skeletal homeostasis in mice. Cell Metabol 2010;11(2):136–46. https://doi.org/10.1016/j.cmet.2009.12.009.
[38] Rached MT, Kode A, Xu L, Yoshikawa Y, Paik JH, Depinho RA, et al. FoxO1 is a positive regulator of bone formation by favoring protein synthesis and resistance to oxidative stress in osteoblasts. Cell Metabol 2010;11(2):147–60. https://doi.org/10.1016/j.cmet.2010.01.001.
[39] Nagao M, Cheong CW, Olsen BR. Col2-Cre and tamoxifen-inducible Col2-CreER target different cell populations in the knee joint. Osteoarthritis Cartilage 2016;24(1):188–91. https://doi.org/10.1016/j.joca.2015.07.025.
[40] Ramasamy SK, Kusumbe AP, Wang L, Adams RH. Endothelial Notch activity promotes angiogenesis and osteogenesis in bone. Nature 2014;507(7492):376–80. https://doi.org/10.1038/nature13146.
[41] Dharaneeswaran H, Abid MR, Yuan L, Dupuis D, Beeler D, Spokes KC, et al. FOXO1-mediated activation of Akt plays a critical role in vascular homeostasis. Circ Res 2014;115(2):238–51. https://doi.org/10.1161/circresaha.115.303227.
[42] Hosaka T, Biggs 3rd WH, Tieu D, Boyer AD, Varki NM, Cavenee WK, et al. Disruption of forkhead transcription factor (FOXO) family members in mice reveals their functional diversification. Proc Natl Acad Sci U S A 2004;101(9):2975–80. https://doi.org/10.1073/pnas.0400093101.
[43] Eguchi J, Wang X, Yu S, Kershaw EE, Chiu PC, Dushay J, et al. Transcriptional control of adipose lipid handling by IRF4. Cell Metabol 2011;13(3):249–59. https://doi.org/10.1016/j.cmet.2011.02.005.
[44] Shi L, Tao Z, Zheng L, Yang J, Hu X, Scott K, et al. FoxO1 regulates adipose transdifferentiation and iron influx by mediating Tgfβ1 signaling pathway. Redox Biol 2023;63:102727. https://doi.org/10.1016/j.redox.2023.102727.
[45] Shi L, Yang J, Tao Z, Zheng L, Bui TF, Alonso RL, et al. Loss of FoxO1 activates an alternate mechanism of mitochondrial quality control for healthy adipose browning. Clin Sci (Lond) 2024;138(6):371–85. https://doi.org/10.1042/cs20230973.
[46] Gao H, Zhong Y, Lin S, Yan Q, Zou X, Xiao G. Bone marrow adipoq(+) cell population controls bone mass via sclerostin in mice. Signal Transduct Targeted Ther 2023;8(1):265. https://doi.org/10.1038/s41392-023-01461-0.
[47] Huang T, Lu Z, Wang Z, Cheng L, Gao L, Gao J, et al. Targeting adipocyte ESRRA promotes osteogenesis and vascular formation in adipocyte-rich bone marrow. Nat Commun 2024;15(1):3769. https://doi.org/10.1038/s41467-024-48255-8.
[48] Yu W, Zhong L, Yao L, Wei Y, Gui T, Li Z, et al. Bone marrow adipogenic lineage precursors promote osteoclastogenesis in bone remodeling and pathologic bone loss. J Clin Invest 2021;131(2). https://doi.org/10.1172/jci140214.
[49] Inoue K, Qin Y, Xia Y, Han J, Yuan R, Sun J, et al. Bone marrow Adipoq-lineage progenitors are a major cellular source of M-CSF that dominates bone marrow macrophage development, osteoclastogenesis, and bone mass. Elife 2023;12. https://doi.org/10.7554/eLife.82118.
[50] Zhong L, Lu J, Fang J, Yao L, Yu W, Gui T, et al. Csf1 from marrow adipogenic precursors is required for osteoclast formation and hematopoiesis in bone. Elife 2023;12. https://doi.org/10.7554/eLife.82112.
[51] Armulik A, Genové G, Betsholtz C. Pericytes: developmental, physiological, and pathological perspectives, problems, and promises. Dev Cell 2011;21(2):193–215. https://doi.org/10.1016/j.devcel.2011.07.001.
[52] Cossutta M, Darche M, Carpentier G, Houppe C, Ponzo M, Raineri F, et al. Weibel-palade bodies orchestrate pericytes during angiogenesis. Arterioscler Thromb Vasc Biol 2019;39(9):1843–58. https://doi.org/10.1161/atvbaha.119.313021.
[53] Zhang Y, Liu J, Zou T, Qi Y, Yi B, Dissanayaka WL, et al. DPSCs treated by TGF-β1 regulate angiogenic sprouting of three-dimensionally co-cultured HUVECs and DPSCs through VEGF-Ang-Tie2 signaling. Stem Cell Res Ther 2021;12(1):281. https://doi.org/10.1186/s13287-021-02349-y.
[54] Chen J, Sivan U, Tan SL, Lippo L, De Angelis J, Labella R, et al. High-resolution 3D imaging uncovers organ-specific vascular control of tissue aging. Sci Adv 2021;7(6). https://doi.org/10.1126/sciadv.abd7819.
[55] Johnston PB, LaPlant B, McPhail E, Habermann TM, Inwards DJ, Micallef IN, et al. Everolimus combined with R-CHOP-21 for new, untreated, diffuse large B-cell lymphoma (NCCTG 1085 [Alliance]): safety and efficacy results of a phase 1 and feasibility trial. Lancet Haematol 2016;3(7):e309–16. https://doi.org/10.1016/s2352-3026(16)30040-0.
[56] Naing A, Aghajanian C, Raymond E, Olmos D, Schwartz G, Oelmann E, et al. Safety, tolerability, pharmacokinetics and pharmacodynamics of AZD8055 in advanced solid tumours and lymphoma. Br J Cancer 2012;107(7):1093–9. https://doi.org/10.1038/bjc.2012.368.
[57] Carosi JM, Sargeant TJ. Rapamycin and Alzheimer disease: a hypothesis for the effective use of rapamycin for treatment of neurodegenerative disease. Autophagy 2023:1–5. https://doi.org/10.1080/15548627.2023.2175569.
[58] Palma JA, Martinez J, Millar Vernetti P, Ma T, Perez MA, Zhong J, et al. mTOR inhibition with sirolimus in multiple system atrophy: a randomized, double-blind, placebo-controlled futility trial and 1-year biomarker longitudinal analysis. Mov Disord 2022;37(4):778–89. https://doi.org/10.1002/mds.28923.
[59] Fitter S, Matthews MP, Martin SK, Xie J, Ooi SS, Walkley CR, et al. mTORC1 plays an important role in skeletal development by controlling preosteoblast differentiation. Mol Cell Biol 2017;37(7). https://doi.org/10.1128/mcb.00668-16.
[60] Xian L, Wu X, Pang L, Lou M, Rosen CJ, Qiu T, et al. Matrix IGF-1 maintains bone mass by activation of mTOR in mesenchymal stem cells. Nat Med 2012;18(7):1095–101. https://doi.org/10.1038/nm.2793.
[61] Liu Q, Liu C, Yang Y, Yang H, Chen J. Osteocyte-intrinsic mTORC1 signaling restrains trabecular bone accrual in mice. J Cell Biochem 2018;119(11):8743–9. https://doi.org/10.1002/jcb.27470.
[62] Wu J, Wang A, Wang X, Li G, Jia P, Shen G, et al. Rapamycin improves bone mass in high-turnover osteoporosis with iron accumulation through positive effects on osteogenesis and angiogenesis. Bone 2019;121:16–28. https://doi.org/10.1016/j.bone.2018.12.019.